The maternal microbiome modulates fetal neurodevelopment in mice

https://doi.org/10.1038/s41586-020-2745-3

Received: 23 July 2019

Accepted: 24 August 2020

Published online: 23 September 2020

Check for updates

Helen E. Vuong[1]✉, Geoffrey N. Pronovost[1], Drake W. Williams[2], Elena J. L. Coley[1], Emily L. Siegler[1], Austin Qiu[1], Maria Kazantsev[1], Chantel J. Wilson[1], Tomiko Rendon[1] & Elaine Y. Hsiao[1]

'Dysbiosis' of the maternal gut microbiome, in response to challenges such as infection[1], altered diet[2] and stress[3] during pregnancy, has been increasingly associated with abnormalities in brain function and behaviour of the offspring[4]. However, it is unclear whether the maternal gut microbiome influences neurodevelopment during critical prenatal periods and in the absence of environmental challenges. Here we investigate how depletion and selective reconstitution of the maternal gut microbiome influences fetal neurodevelopment in mice. Embryos from antibiotic-treated and germ-free dams exhibited reduced brain expression of genes related to axonogenesis, deficient thalamocortical axons and impaired outgrowth of thalamic axons in response to cell-extrinsic factors. Gnotobiotic colonization of microbiome-depleted dams with a limited consortium of bacteria prevented abnormalities in fetal brain gene expression and thalamocortical axonogenesis. Metabolomic profiling revealed that the maternal microbiome regulates numerous small molecules in the maternal serum and the brains of fetal offspring. Select microbiota-dependent metabolites promoted axon outgrowth from fetal thalamic explants. Moreover, maternal supplementation with these metabolites abrogated deficiencies in fetal thalamocortical axons. Manipulation of the maternal microbiome and microbial metabolites during pregnancy yielded adult offspring with altered tactile sensitivity in two aversive somatosensory behavioural tasks, but no overt differences in many other sensorimotor behaviours. Together, our findings show that the maternal gut microbiome promotes fetal thalamocortical axonogenesis, probably through signalling by microbially modulated metabolites to neurons in the developing brain.

The microbiome is an important modulator of brain function and behaviour[4]. Animals reared devoid of microbial colonization (germ-free, GF) or depleted of the microbiome (antibiotic-treated, ABX) exhibit altered neurophysiology and behaviour compared to conventionally colonized (specific pathogen-free, SPF) controls. Only a subset of phenotypes can be corrected by restoring the microbiome postnatally, suggesting that the maternal gestational microbiome is involved in the regulation of developmental processes that affect brain function and behaviour in adulthood. Indeed, the gut microbiome is required to mediate the ability of maternal challenges, such as immune activation[1], a high fat diet[2] and psychosocial stress[3], to induce neurobehavioural abnormalities in mice. It remains unclear, however, whether such microbial influences on neurodevelopment originate antenatally, via disrupted function of the maternal microbiota, and/or postnatally, via vertically transmitted alterations in the neonatal microbiota[5]. Moreover, although it has been shown that the maternal microbiome can modulate host responses to acute insults, it is unclear whether it affects the development of offspring in the absence of environmental challenges. Herein, we examine roles for the maternal gut microbiome during homeostasis in regulating early embryonic brain development and later-life behaviour of the offspring.

The maternal microbiota promotes axonogenesis

To determine whether the maternal microbiome influences fetal neurodevelopment, we first examined fetal brains from the offspring of female mice that were reared SPF or GF, or treated with ABX to deplete the maternal microbiome from before conception through mid-gestation. Depletion of the maternal microbiome altered the expression of 333 genes in the brains of embryos at embryonic day 14.5 (E14.5), including many genes involved in axonogenesis (Fig. 1a, Supplementary Table 1, Extended Data Fig. 1a, c, d). Netrin-G1a (encoded by *NTNG1*), a glycosylphosphatidylinositol-tethered protein that is expressed by developing thalamocortical axons[6], was downregulated in fetal brains in the offspring of ABX and GF dams (Fig. 1a, Extended Data Fig. 1b). Consistent with reductions in *NTNG1* transcription, fetal brains from offspring of ABX and GF dams exhibited reduced netrin-G1a^{+} immunoreactivity localized to thalamocortical axons at E14.5 (Fig. 1b,

[1]Department of Integrative Biology and Physiology, University of California Los Angeles, Los Angeles, CA, USA. [2]Oral Immunity and Inflammation Section, NIDCR, NIH, Bethesda, MD, USA. ✉e-mail: hvuong2323@gmail.com

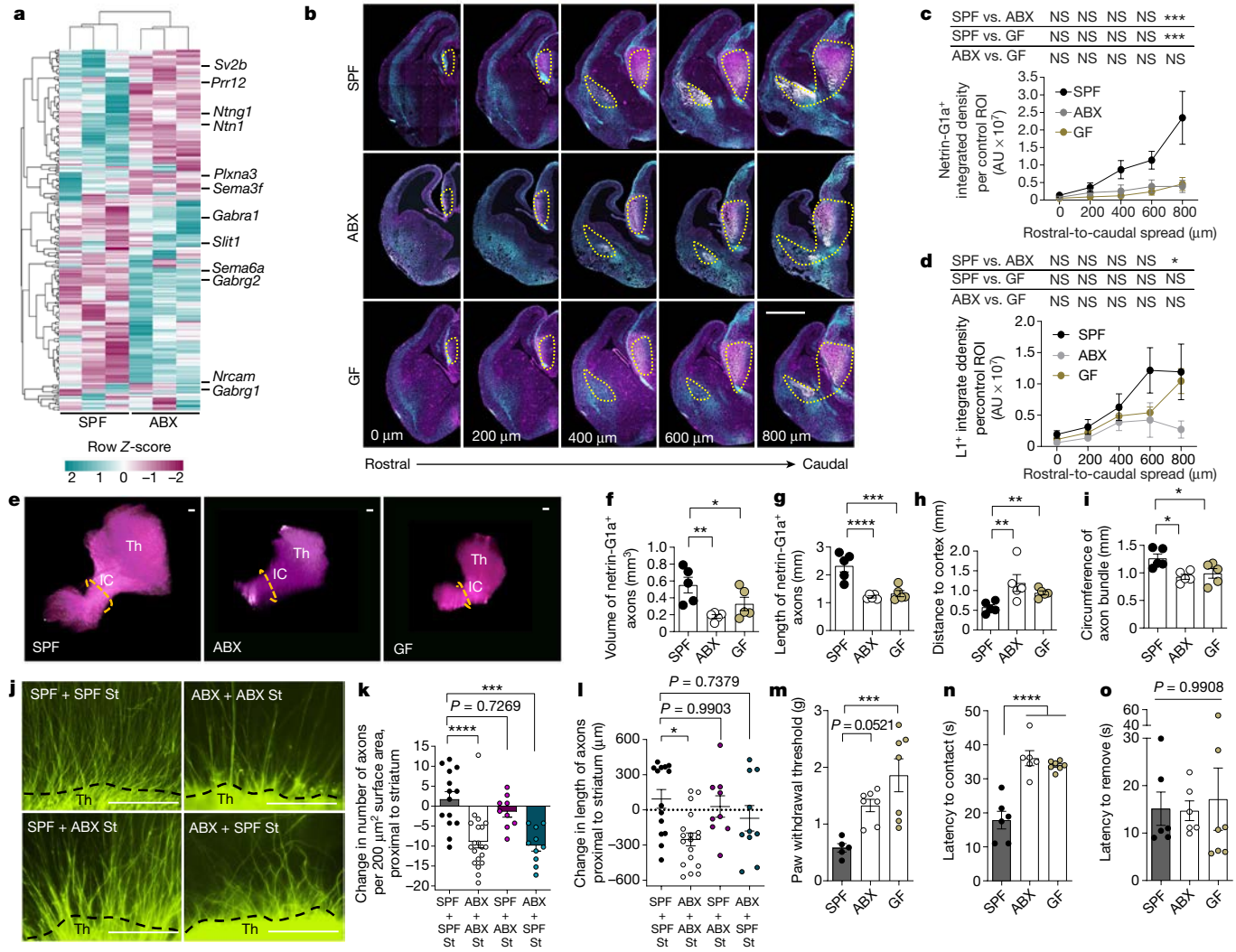

Fig. 1 | Depletion of the maternal microbiome impairs fetal thalamocortical axonogenesis. a, Genes that are differentially expressed in E14.5 brains from offspring of SPF and ABX dams (two-tailed Wald, $P < 0.05$, $n = 3$ dams). Axonogenesis-related genes are highlighted. **b**, Netrin-G1a (magenta) and L1 (cyan) in E14.5 brains from SPF, ABX and GF dams. Scale bar, 500 µm. Yellow lines, control ROIs. **c**, **d**, Netrin-G1a (**c**) and L1 (**d**) fluorescence per matched control ROI in E14.5 brain sections (two-way ANOVA and Tukey's test, $n = 5$ offspring from different dams). AU, arbitrary units. **e**, Netrin-G1a in whole E14.5 brains. Scale bars, 100 µm. Th, thalamus; IC, internal capsule. Dotted line, axon bundle circumference. **f**–**i**, In whole E14.5 brains, netrin-G1a$^+$ axonal volume (**f**), axon length (**g**), distance from rostral tip to cortex (**h**) and circumference of the axon bundle at internal capsule (**i**) (SPF versus ABX: one-way ANOVA with Tukey's test; SPF versus GF: one-tailed Mann–Whitney test; $n = 5$ offspring from different dams). **j**, TUJ1$^+$ axons from SPF thalamus and SPF striatum (top left), ABX thalamus and ABX striatum (top right), SPF thalamus and ABX striatum (bottom left) and ABX thalamus and SPF striatum (bottom right). Scale bars, 250 µm. **k**, **l**, Axons per 200 µm^2 surface area proximal to striatum (**k**) and length of thalamic axons proximal to striatum (**l**), normalized to thalamic monoculture (two-way ANOVA and Tukey's test, $n = 14, 20, 9, 10$ from left to right). **m**–**o**, Behaviour in adult offspring of SPF, ABX, and GF dams. **m**, Force filament to induce 50% paw withdrawal (one-way ANOVA with Tukey's test, $n = 5, 7, 7$ dams). **n**, **o**, Latency to contact the adhesive (**n**) and latency to remove the adhesive after first contact (**o**) (one-way ANOVA and Tukey's test, $n = 6, 6, 7$ dams). Mean ± s.e.m., $^*P < 0.05$, $^{**}P < 0.01$, $^{***}P < 0.001$, $^{****}P < 0.0001$, NS, not statistically significant.

c, Extended Data Fig. 2a–k, Supplementary Discussion). Evaluation of netrin-G1a$^+$ thalamocortical axons in cleared whole brains similarly revealed decreased axonal volume and length in E14.5 offspring from microbiome-depleted dams (Fig. 1e–i). The alterations in netrin-G1a expression were maintained after the data were normalized to observed reductions in whole brain volume, which suggests that decreases in netrin-G1a are not solely a function of variation in brain size (Extended Data Fig. 3a–f, Supplementary Discussion). Fetal brains from the offspring of ABX dams also showed decreased expression of neural cell adhesion molecule L1, a pan-axonal marker (Fig. 1b, d, Extended Data Fig. 3g–i), with no significant differences in DAPI-positive cell counts in the thalamus (Extended Data Fig. 2l, m). This suggests that reductions in netrin-G1a reflect decreases in thalamocortical projections, rather than diminished receptor expression on existing axons or the absence of thalamic neurons themselves. Overall, these results suggest that the maternal microbiome is required to support fetal thalamocortical axonogenesis in the developing mouse offspring.

Axonogenesis involves cell-intrinsic and cell-extrinsic factors that work together to direct axon polarity, elongation and pathfinding. To determine whether the reduction in netrin-G1a$^+$ thalamocortical axons seen in response to maternal microbiome depletion was due to impaired axon formation, deficient axon guidance or both, we cultured thalamic explants, either alone or in the presence of endogenous cues from striatal and hypothalamic explants[7]. Monoculture of thalamic explants from E14.5 offspring of either SPF or ABX dams resulted in substantial axon outgrowth (Extended Data Fig. 4a–c),

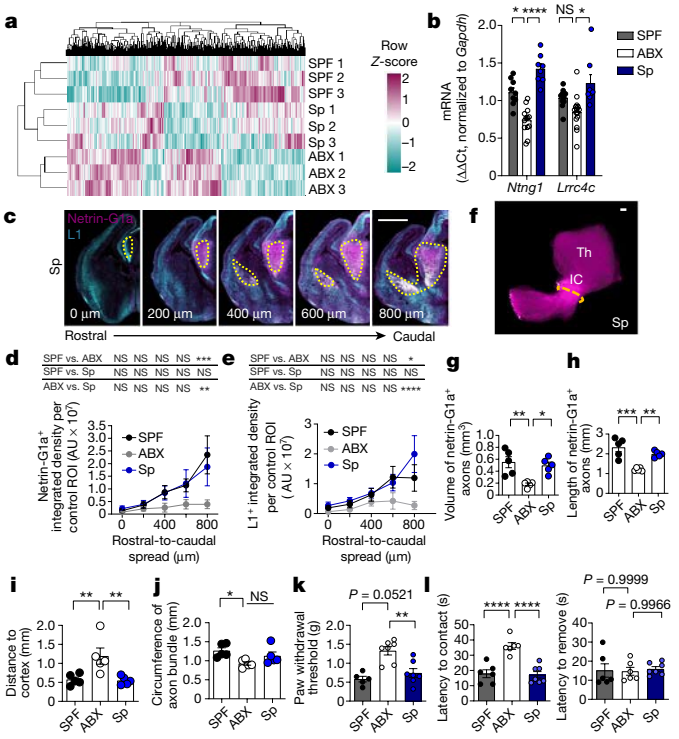

Fig. 2 | Colonization of the maternal microbiota prevents neurodevelopmental abnormalities induced by microbiome depletion. a, Differentially expressed genes in E14.5 brains of offspring from SPF, ABX and Sp-colonized dams (two-tailed Wald, $n = 3$ dams). **b**, *Ntng1* and *Lrrc4c* mRNA expression normalized to the expression of *Gapdh* mRNA in E14.5 brains (two-way ANOVA and Tukey's test, $n = 9, 13, 8$ offspring from different dams for SPF, ABX and Sp, respectively). **c**, Netrin-G1a (magenta) and L1 (cyan) in E14.5 Sp brain sections. Scale bar, 500 µm. **d**, **e**, Netrin-G1a (**d**) and L1 (**e**) fluorescence per matched ROI in E14.5 brain sections (two-way ANOVA and Tukey's test, $n = 5$ offspring from different dams). **f**, Netrin-G1a in whole E14.5 brain from an Sp-colonized dam. Scale bar, 100 µm. **g**–**j**, Volume (**g**) and length (**h**) of netrin-G1a axons, distance from distal tip of netrin-G1a axons to cortex (**i**) and circumference of netrin-G1a axonal bundle at the internal capsule (**j**) in whole E14.5 brains (one-way ANOVA and Tukey's test; $n = 5$ offspring from different dams). **k**, Force filament to induce 50% paw withdrawal in adult offspring (one-way ANOVA and Tukey's test, $n = 5, 7, 7$ dams). **l**, Left, forepaw sensitivity, as latency to contact adhesive tape, in adult offspring; right, forepaw motor dexterity, as latency to remove the adhesive tape after first contact, in adult offspring (one-way ANOVA and Tukey's test, $n = 6, 6, 7$ dams). Mean ± s.e.m. SPF and ABX data are as displayed in Fig. 1, Extended Data Figs. 2–4. $^*P < 0.05$, $^{**}P < 0.01$, $^{***}P < 0.001$, $^{****}P < 0.0001$, NS, not statistically significant.

suggesting that the reductions in netrin-G1a$^+$ axons seen in the embryos of microbiome-depleted dams are not due to an intrinsic inability of the thalamus to form or elongate axons. Indeed, thalamic neurons from embryos of ABX dams generated increased numbers of axons, with no significant difference in axon length, as compared to SPF controls (Extended Data Fig. 4a–c); this suggests an enhanced capacity for axon formation, but not elongation, in fetal thalamic neurons from ABX dams that are grown in rich medium. However, when co-cultured with fetal striatal and hypothalamic explants from ABX dams, fetal thalamic neurons from embryos of ABX dams exhibited impaired axon outgrowth, with a decreased number and length of axons as compared to co-cultured control explants from offspring of SPF mothers (Fig. 1j–l, white versus black). These abnormalities in cue-regulated axonal outgrowth were observed for thalamic axons proximal to the striatal explant (Fig. 1j–l), which produces growth-promoting and attractive guidance cues[8], as well as for axons proximal to the hypothalamic explant (Extended Data Fig. 4d–f), which produces growth-inhibiting and repulsive guidance cues[9]. Analogous deficits in the number of axons, but not the lengths of axons, were seen in fetal thalamic explants from the offspring of GF dams (Extended Data Fig. 4g–l). These discrepancies could be due to confounding effects of maternal GF rearing or ABX exposure. Together, these results indicate that fetal thalamic neurons from E14.5 offspring of microbiota-deficient dams display impaired axon outgrowth when co-cultured with corresponding striatal and hypothalamic explants, but not when grown alone in monoculture. This suggests that depletion of the maternal microbiome disrupts fetal thalamic responses to tissue-derived factors in mice.

To gain further insight into whether depletion of the maternal microbiome alters tissue-derived cues to impair axon outgrowth, we co-cultured fetal thalamic explants from embryos of SPF or ABX dams with striatal and hypothalamic explants from the contrasting experimental group. When thalamic explants from embryos of SPF dams were co-cultured with striatal and hypothalamic explants from embryos of ABX dams, there were no significant differences in the number or length of axons from SPF thalamic neurons (Fig. 1j–l, purple versus black, Extended Data Fig. 4d–f). This suggests that ABX tissue-derived factors sufficiently support axon outgrowth from SPF thalamic neurons. By contrast, when thalamic explants from embryos of ABX dams were co-cultured with striatal and hypothalamic explants from embryos of SPF dams, ABX thalamic neurons exhibited deficiencies in axon outgrowth, at levels similar to those seen in response to co-culture with ABX tissues (Fig. 1j–l, Extended Data Fig. 4d–f, teal versus white). This suggests that endogenous soluble factors from SPF explants are not sufficient to correct impairments in axon outgrowth from ABX thalamic neurons, and that ABX thalamic neurons respond incorrectly to factors from SPF tissues. Such thalamus-intrinsic alterations in responsivity to cues could be attributed to erroneously repulsive responses to attractive guidance cues[10], hyperresponsiveness to repulsive cues[11] and/or cue-induced disruptions in thalamic responses to neurotrophic factors present in the culture medium[12]. Overall, these findings indicate that tissue-derived cues are necessary but not sufficient for mediating maternal microbiota-dependent reductions in thalamic axonogenesis and further suggest that depletion of the maternal microbiome impairs the complex interactions between intrinsic and extrinsic factors that regulate responses of fetal thalamocortical neurons to axonogenic cues in mice.

Thalamocortical axons are guided to the somatosensory cortex, where they form dense synaptic contacts with neurons to mediate sensory processing[13]. To gain insight into whether microbiome-induced alterations in fetal thalamocortical axonogenesis confer lasting influences on offspring behaviour, SPF dams were treated with ABX or vehicle from pre-conception through E14.5, and then re-colonized with SPF microbiota for the remainder of gestation through postnatal development (Extended Data Fig. 5, Supplementary Table 2). Conventionalized adult offspring of GF, ABX or vehicle-treated dams were tested in a battery of sensory behavioural tasks (Fig. 1m–o, Extended Data Fig. 6, Supplementary Table 3). In the von Frey filament test for hindpaw sensorimotor function[14], adult offspring of ABX and GF dams required increased force thresholds for paw withdrawal in response to hindpaw stimulation than did control offspring from SPF dams (Fig. 1m, Extended Data Fig. 6b, g), suggesting that their tactile sensation was impaired. Consistent with this, in the adhesive removal test for forepaw sensorimotor function[15], adult offspring of ABX and GF dams exhibited increased latency to detect and contact the forepaw stimulus compared to control offspring from SPF dams (Fig. 1n, Extended Data Fig. 6c, e, h). There was no difference in the time to remove the adhesive after first contact, suggesting that ABX and GF offspring exhibit deficient paw tactile sensation, but no disruption in motor response (Fig. 1o, Extended Data Fig. 6d, e, i). Adult offspring of GF dams also exhibited modest alterations in thermosensory behaviour[16] and acoustic sensorimotor behaviour[17] (Extended Data Fig. 6j–l). The phenotypes were inconsistent between GF and ABX conditions, suggesting nuanced

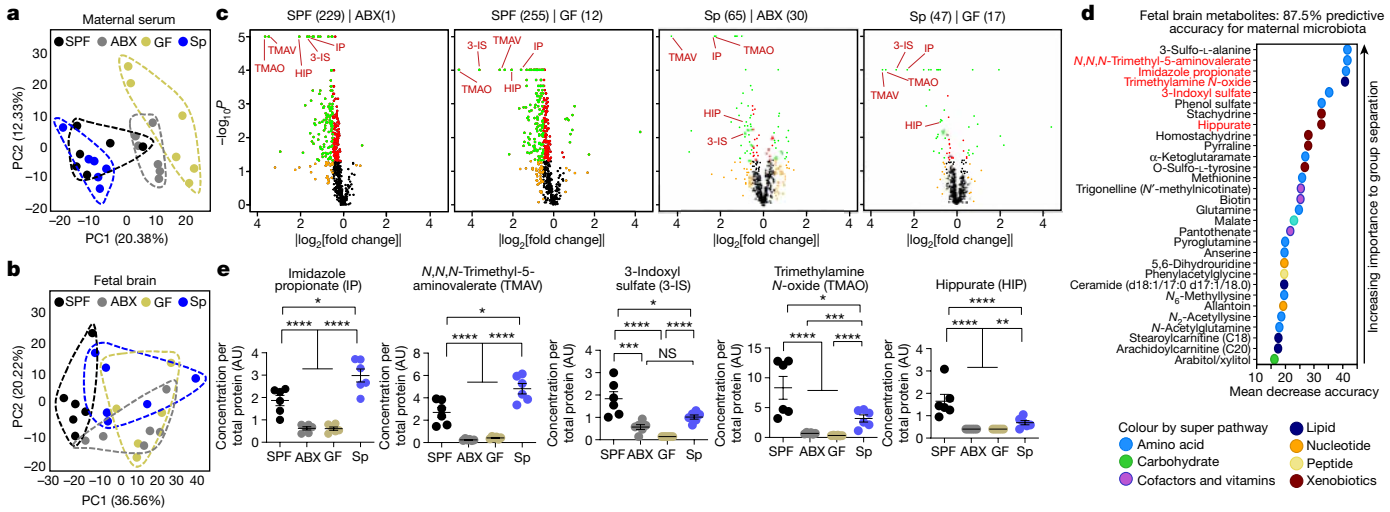

Fig. 3 | The maternal microbiota modulates maternal serum and fetal brain metabolites during pregnancy. a, Principal component (PC) analysis of maternal serum metabolomes from SPF, ABX, GF and Sp-colonized dams on E14.5 ($n = 6$ dams) **b**, Principal component analysis of 567 metabolites detected in fetal brain metabolomes from E14.5 offspring of SPF, ABX, GF and Sp-colonized dams ($n = 6$ embryos from different dams). **c**, Significantly regulated E14.5 fetal brain metabolites. Orange, $\log_2$[fold change] > 0.5; red, $P < 0.05$; green, $\log_2$[fold change] > 0.5 and $P < 0.05$. Parentheses denote the number of significantly elevated metabolites in each group pairwise comparison (one-way ANOVA with FDR contrasts, $n = 6$ embryos from different dams). **d**, Random forest classification of top 30 metabolites in E14.5 fetal brain that discriminate between offspring of SPF and Sp-colonized dams versus ABX and GF dams. Red, at least twofold decrease in ABX and GF compared with SPF and Sp ($n = 6$ embryos from different dams). **e**, Select metabolites that are significantly decreased in E14.5 fetal brains from embryos of ABX and GF dams versus SPF and Sp-colonized dams (one-way ANOVA with FDR contrasts, $n = 6$ embryos from different dams). Mean ± s.e.m. *$q < 0.05$, **$q < 0.01$, ***$q < 0.001$, ****$q < 0.0001$, NS, not statistically significant.

developmental effects that differ between chronic GF rearing and acute ABX exposure. Notably, there were no apparent differences between ABX, GF and control SPF offspring in tests for visual sensory behaviour[18], vibrissae sensory perception[19] or motor coordination[20] (Extended Data Fig. 6m–o). This suggests that maternal microbial effects are somewhat specific to adult tactile sensory circuits. This specificity may be attributed to selective recovery of thalamocortical circuits for other sensory modalities, the need for more sensitive behavioural assays that adequately quantify abnormalities in other sensory modalities, and/or the possibility that the observed sensory behavioural phenotypes are due to microbiome-dependent defects elsewhere in the nervous system, aside from thalamocortical neurons. Together, these results show that depletion of the maternal gut microbiota during early to mid-gestation in mice impairs fetal thalamocortical axonogenesis and yields adult offspring with disrupted neurobehavioural responses to forepaw and hindpaw tactile stimuli.

Select bacteria prevent axonal defects

The gut microbiome comprises various microbial taxa that interact differently with host physiology. To determine whether the effects of the maternal microbiota on offspring neurodevelopment and behaviour are mediated by particular bacteria, we colonized ABX-treated dams during pre-conception with bacterial consortia representing the two dominant phyla—Firmicutes and Bacteroidetes (Extended Data Fig. 7a–c, h–j, Supplementary Tables 4, 5). Colonization of ABX dams with *Clostridia*-dominant spore-forming (Sp) bacteria abrogated many of the adverse effects of maternal microbiota depletion on fetal brain gene expression and thalamocortical axonogenesis (Fig. 2a, Extended Data Fig. 7d–g, Supplementary Table 1). Reductions in *NTNG1* expression and netrin-G1a$^+$ thalamocortical axons were prevented by maternal colonization with Sp bacteria (Fig. 2b–j, Extended Data Fig. 1). By contrast, maternal colonization with a consortium of *Bacteroides* species (BD) conferred only a modest increase in netrin-G1a$^+$ thalamocortical axons and had no effect on L1$^+$ thalamocortical axons (Extended Data Fig. 7k–m). Maternal colonization with BD bacteria yielded faecal microbiota with about 95% relative abundance of *Bacteroides* species and about 5% of an operational taxonomic unit (OTU) that mapped to *Clostridium difficile*, which may also contribute to this partial restoration (Extended Data Fig. 7h–m, Supplementary Table 5). Fetal thalamic explants from E14.5 embryos of Sp-colonized dams exhibited increased axon outgrowth compared to ABX controls (Extended Data Fig. 4m–r). Deficiencies in paw tactile sensory behaviour were prevented by maternal colonization with Sp bacteria (Fig. 2k, l, Extended Data Fig. 6a–i). Overall, these findings suggest that certain bacterial taxa, including Sp bacteria in particular, are sufficient to prevent the adverse effects of maternal microbiome deficiency on fetal thalamocortical axonogenesis and offspring tactile sensory behaviour in mice.

Maternal microbes shape the fetal metabolome

The gut microbiota modulates the bioavailability of hundreds of biochemicals in the circulating blood[21]. During pregnancy, nutrients and growth factors from the maternal blood support offspring growth, and this is particularly important for the permeable[22] and rapidly developing fetal brain[23]. On the basis of our finding that the maternal microbiome is important for regulating fetal neurodevelopment in mice, we hypothesized that the maternal microbiota regulates circulating metabolites and thereby conditions metabolite profiles in the fetus. To investigate this, we profiled biochemicals in maternal sera and fetal brain lysates from SPF, ABX, GF and Sp-colonized dams on E14.5. We identified 753 metabolites in maternal sera and 567 in fetal brain lysates (Supplementary Tables 6, 7). Maternal serum metabolomic profiles from SPF and Sp-colonized dams were more similar than those from GF and ABX dams (Fig. 3a, Extended Data Fig. 8a, d, e). This suggests that Sp colonization recapitulates many effects of the SPF microbiota on maternal biochemical profiles, and aligns with the phenotypic similarities between offspring of ABX and GF dams versus SPF and Sp-colonized dams in fetal axonogenesis and adult tactile sensory behaviour. Brain lysates from E14.5 embryos of microbiome-depleted dams also exhibited altered metabolite profiles relative to those from SPF and Sp dams (Fig. 3b–e, Extended Data Fig. 8b, c, Supplementary

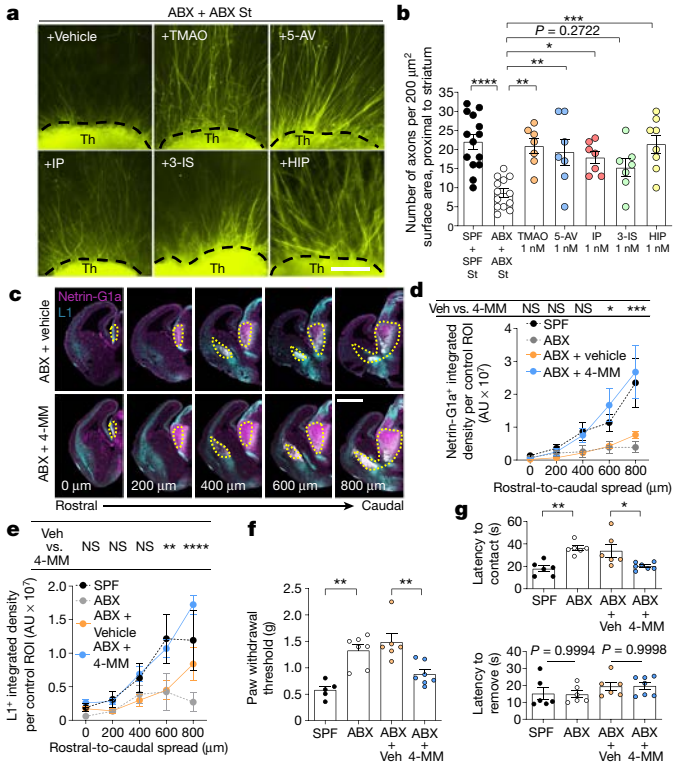

Fig. 4 | The maternal microbiota modulates metabolites that promote fetal thalamocortical axonogenesis. a, Axon outgrowth from ABX thalamic explants proximal to ABX striatal explants, supplemented with vehicle, TMAO (1 nM), 5-AV (1 nM), IP (1 nM), 3-IS (1 nM) or HIP (1 nM). Scale bar, 250 µm. **b**, Number of axons per 200 µm² surface area proximal to striatal explant (one-way ANOVA and Tukey's test, $n = 14, 13, 7, 7, 7, 7, 8$ from left to right). **c**, Netrin-G1a (magenta) and L1 (cyan) in E14.5 brain sections from offspring of ABX dams treated with vehicle or 4-MM (TMAO, 5-AV, IP and HIP). Scale bar, 500 µm. **d**, **e**, Netrin-G1a (**d**) and L1 (**e**) per matched ROI (yellow dashed outlines in **c**) in E14.5 brain sections from offspring of vehicle- or 4-MM-treated ABX dams (two-way ANOVA and Tukey's test, $n = 8$ offspring from different dams). **f**, Force filament to induce 50% paw withdrawal in adult offspring of SPF, ABX, ABX + veh, and ABX + 4-MM dams (one-way ANOVA and Tukey's test, $n = 5, 7, 6, 7$ dams). **g**, Top, latency to contact the adhesive in adult offspring of SPF, ABX, ABX + veh, and ABX + 4-MM dams. Bottom, latency to remove the adhesive after first contact in offspring of SPF, ABX, ABX + veh, and ABX + 4-MM dams (one-way ANOVA and Tukey's test, $n = 6, 6, 6, 7$ dams). Behavioural data for SPF and ABX as reference controls are as in Figs. 1, 2. Mean ± s.e.m. $^{*}P < 0.05$, $^{**}P < 0.01$, $^{***}P < 0.001$, $^{****}P < 0.0001$, NS, not statistically significant.

Table 6). Thirty fetal brain metabolites predicted maternal microbiota status (SPF and Sp versus ABX and GF) with 87.5% accuracy (Fig. 3d). Twenty-two metabolites were similarly and significantly decreased in fetal brain lysates from ABX and GF dams relative to both SPF and Sp-colonized dams (Supplementary Table 7). Of these 22 fetal brain metabolites, 8 were similarly differentially regulated in maternal sera from ABX and GF dams compared to SPF and Sp-colonized controls (Supplementary Table 7), suggesting that the maternal microbiota modulates the bioavailability of these metabolites in maternal blood and has direct effects on the bioavailability of the same metabolites in the fetal brain. These findings reveal that the maternal microbiota regulates biochemical profiles and select metabolites in the fetal brains of developing offspring.

Select metabolites promote axonogenesis

To determine whether particular metabolites mediate the ability of the maternal microbiome to promote fetal thalamocortical axonogenesis in mice, we exposed thalamic explants from E14.5 embryos of ABX-treated dams to select metabolites and evaluated their axon outgrowth. The metabolites trimethylamine-*N*-oxide (TMAO), *N*,*N*,*N*-trimethyl-5-aminovalerate (TMAV), imidazole propionate (IP), 3-indoxyl sulfate (3-IS) and hippurate (HIP) were selected because they showed a more than twofold reduction in both maternal blood and fetal brain from ABX and GF dams, relative to SPF controls, and were elevated following the colonization of dams with Sp bacteria (Fig. 3e, Extended Data Fig. 10f). In addition, each metabolite is regulated in adult stool, blood and/or prefrontal cortex by the gut microbiota[21,24,25]. Fetal thalamic explants from E14.5 embryos of ABX dams showed impaired axonogenesis in response to co-culture with ABX striatal and hypothalamic explants (Fig. 1j–l). Exposure to physiological concentrations of TMAO, 5-aminovalerate (5-AV, a reported precursor to TMAV), IP or HIP, but not 3-IS, increased axon numbers to the levels seen in fetal brain explants from embryos of SPF dams (Fig. 4a, b, Extended Data Fig. 9a). 5-AV and IP also increased axon length, whereas TMAO and 3-IS induced modest but not statistically significant increases, and HIP had no effect (Extended Data Fig. 9b). Thalamic explants from offspring of GF dams responded similarly, with TMAO, IP and HIP increasing axon outgrowth (Extended Data Fig. 9e–i). No significant changes were found in the number and length of thalamic axons from offspring of ABX dams proximal to the hypothalamus (Extended Data Fig. 9c, d).

To further test whether maternal metabolite supplementation affects fetal neurodevelopment in vivo, ABX-treated dams were injected intraperitoneally with TMAO, 5-AV, IP and HIP (4-MM) or vehicle from E7 to E14 of gestation, the developmental time frame during which thalamocortical axonogenesis occurs[26] (Extended Data Fig. 6p). Maternal supplementation with 4-MM prevented the reductions in netrin-G1a^{+} thalamocortical axons seen in offspring of microbiome-depleted dams (Fig. 4c–e, Extended Data Fig. 10a–d). By contrast, maternal supplementation with the short chain fatty acids propionate, butyrate and acetate had no significant effect on fetal thalamocortical axons (Extended Data Fig. 10g–n). Maternal supplementation with 4-MM significantly increased the levels of TMAO and IP, but not TMAV, 3-IS or HIP, in the fetal brain, compared to vehicle-supplemented controls (Extended Data Fig. 10e). These results suggest that elevations in TMAO and IP, in particular, may mediate the effects of 4-MM on promoting thalamocortical axonogenesis in vivo. Consistent with this, maternal colonization with BD, which did not substantially promote netrin-G1a^{+} thalamocortical axons (Extended Data Fig. 7k–m), had no overt effect on the levels of TMAO and IP, but elevated TMAV and 3-IS in the fetal brain (Extended Data Fig. 10f). Furthermore, adult offspring of ABX dams that were supplemented with 4-MM exhibited improvements in tactile sensory behaviour relative to the offspring of vehicle-treated ABX controls (Fig. 4f, g, Extended Data Fig. 6p–w). Together, our results show that the maternal microbiome promotes fetal thalamocortical axonogenesis in mice, probably via microbiota-dependent biochemicals, such as TMAO and IP, in the fetal brain.

Discussion

The gut microbiota modulates numerous bioactive molecules in the intestine, serum and various extraintestinal organs[27]. Our findings reveal that during pregnancy, the maternal gut microbiota regulates metabolites, not only in the maternal compartment, but also in the fetus itself, including the fetal brain. Select fetal brain metabolites that are regulated by the maternal gut microbiota induce axon outgrowth from mouse thalamic explants and promote fetal thalamocortical axonogenesis in offspring of microbiome-depleted dams. Although the molecular mechanisms that underlie the effects of microbial metabolites on neurons remain unclear, some metabolites, such as TMAO, TMAV and HIP, have been associated with neurological conditions and factors related to neurite outgrowth (Supplementary Discussion). In addition, our findings parallel evidence that malnutrition-induced

alterations in the maternal microbiome are associated with reduced white matter in the brains of adolescent and adult offspring[28–31], and that inflammation-induced alterations in the maternal gut microbiota disrupt somatosensory cortical architecture in adult mouse offspring[32]. Furthermore, a recent study of microbiomes in malnourished children reported dysregulation of several proteins associated with axonogenesis, which was ameliorated by treatment with microbiota-directed diets[33]. Several large epidemiological studies have found that maternal infection and use of antibiotics is associated with increased risk for neurodevelopmental complications in offspring[34,35]. However, whether these effects in humans are mediated by alterations in the maternal microbiome remain unclear. Our results support the idea that the maternal microbiome has an important role in promoting neurodevelopment in offspring, and further suggest that interactions between the microbiome and nervous system begin prenatally through influences of the maternal gut microbiota on fetal brain metabolomic profiles and gene expression. Thus, early to mid-gestation is a critical period during which the maternal microbiome promotes fetal neurodevelopment to support developmental processes that may underlie later-life behaviours in mice.

Online content

Any methods, additional references, Nature Research reporting summaries, source data, extended data, supplementary information, acknowledgements, peer review information; details of author contributions and competing interests; and statements of data and code availability are available at https://doi.org/10.1038/s41586-020-2745-3.

1. Kim, S. et al. Maternal gut bacteria promote neurodevelopmental abnormalities in mouse offspring. *Nature* **549**, 528–532 (2017).
2. Buffington, S. A. et al. Microbial reconstitution reverses maternal diet-induced social and synaptic deficits in offspring. *Cell* **165**, 1762–1775 (2016).
3. Jašarević, E. et al. The maternal vaginal microbiome partially mediates the effects of prenatal stress on offspring gut and hypothalamus. *Nat. Neurosci*. **21**, 1061–1071 (2018).
4. Vuong, H. E., Yano, J. M., Fung, T. C. & Hsiao, E. Y. The microbiome and host behavior. *Annu. Rev. Neurosci*. **40**, 21–49 (2017).
5. Ferretti, P. et al. Mother-to-infant microbial transmission from different body sites shapes the developing infant gut microbiome. *Cell Host Microbe* **24**, 133–145.e135 (2018).
6. Nakashiba, T. et al. Netrin-G1: a novel glycosyl phosphatidylinositol-linked mammalian netrin that is functionally divergent from classical netrins. *J. Neurosci*. **20**, 6540–6550 (2000).
7. Rennie, S., Lotto, R. B. & Price, D. J. Growth-promoting interactions between the murine neocortex and thalamus in organotypic co-cultures. *Neuroscience* **61**, 547–564 (1994).
8. Mitsogiannis, M. D., Little, G. E. & Mitchell, K. J. Semaphorin–plexin signaling influences early ventral telencephalic development and thalamocortical axon guidance. *Neural Dev*. **12**, 6 (2017).
9. Braisted, J. E., Ringstedt, T. & O'Leary, D. D. Slits are chemorepellents endogenous to hypothalamus and steer thalamocortical axons into ventral telencephalon. *Cereb. Cortex* **19**, i144–i151 (2009).
10. Song, H. et al. Conversion of neuronal growth cone responses from repulsion to attraction by cyclic nucleotides. *Science* **281**, 1515–1518 (1998).
11. Stevens, A. & Jacobs, J. R. Integrins regulate responsiveness to slit repellent signals. *J. Neurosci*. **22**, 4448–4455 (2002).
12. Dontchev, V. D. & Letourneau, P. C. Nerve growth factor and semaphorin 3A signaling pathways interact in regulating sensory neuronal growth cone motility. *J. Neurosci*. **22**, 6659–6669 (2002).
13. Enriquez-Barreto, L., Palazzetti, C., Brennaman, L. H., Maness, P. F. & Fairén, A. Neural cell adhesion molecule, NCAM, regulates thalamocortical axon pathfinding and the organization of the cortical somatosensory representation in mouse. *Front. Mol. Neurosci*. **5**, 76 (2012).
14. Chaplan, S. R., Bach, F. W., Pogrel, J. W., Chung, J. M. & Yaksh, T. L. Quantitative assessment of tactile allodynia in the rat paw. *J. Neurosci. Methods* **53**, 55–63 (1994).
15. Bouet, V. et al. The adhesive removal test: a sensitive method to assess sensorimotor deficits in mice. *Nat. Protocols* **4**, 1560–1564 (2009).
16. Eddy, N. B. & Leimbach, D. Synthetic analgesics. II. Dithienylbutenyl- and dithienylbutylamines. *J. Pharmacol. Exp. Ther*. **107**, 385–393 (1953).
17. Valsamis, B. & Schmid, S. Habituation and prepulse inhibition of acoustic startle in rodents. *J. Vis. Exp*. **55**, e3446 (2011).
18. Fox, M. W. The visual cliff test for the study of visual depth perception in the mouse. *Anim. Behav*. **13**, 232–233 (1965).
19. Wu, H. P., Ioffe, J. C., Iverson, M. M., Boon, J. M. & Dyck, R. H. Novel, whisker-dependent texture discrimination task for mice. *Behav. Brain Res*. **237**, 238–242 (2013).
20. Deacon, R. M. Measuring motor coordination in mice. *J. Vis. Exp*. **75**, e2609 (2013).
21. Fujisaka, S. et al. Diet, genetics, and the gut microbiome drive dynamic changes in plasma metabolites. *Cell Rep*. **22**, 3072–3086 (2018).
22. Saunders, N. R., Liddelow, S. A. & Dziegielewska, K. M. Barrier mechanisms in the developing brain. *Front. Pharmacol*. **3**, 46 (2012).
23. Monk, C., Georgieff, M. K. & Osterholm, E. A. Research review: maternal prenatal distress and poor nutrition - mutually influencing risk factors affecting infant neurocognitive development. *J. Child Psychol. Psychiatry* **54**, 115–130 (2013).
24. Olson, C. A. et al. The gut microbiota mediates the anti-seizure effects of the ketogenic diet. *Cell* **174**, 497 (2018).
25. Matsumoto, M. et al. Cerebral low-molecular metabolites influenced by intestinal microbiota: a pilot study. *Front. Syst. Neurosci*. **7**, 9 (2013).
26. Molnár, Z., Garel, S., López-Bendito, G., Maness, P. & Price, D. J. Mechanisms controlling the guidance of thalamocortical axons through the embryonic forebrain. *Eur. J. Neurosci*. **35**, 1573–1585 (2012).
27. Vernocchi, P., Del Chierico, F. & Putignani, L. Gut microbiota profiling: metabolomics based approach to unravel compounds affecting human health. *Front. Microbiol*. **7**, 1144 (2016).
28. Lu, J. et al. Microbiota influence the development of the brain and behaviors in C57BL/6J mice. *PLoS One* **13**, e0201829 (2018).
29. Ong, I. M. et al. Gut microbiome populations are associated with structure-specific changes in white matter architecture. *Transl. Psychiatry* **8**, 6 (2018).
30. Indrio, F. et al. Epigenetic matters: the link between early nutrition, microbiome, and long-term health development. *Front Pediatr*. **5**, 178 (2017).
31. Keunen, K., van Elburg, R. M., van Bel, F. & Benders, M. J. Impact of nutrition on brain development and its neuroprotective implications following preterm birth. *Pediatr. Res*. **77**, 148–155 (2015).
32. Shin Yim, Y. et al. Reversing behavioural abnormalities in mice exposed to maternal inflammation. *Nature* **549**, 482–487 (2017).
33. Gehrig, J. L. et al. Effects of microbiota-directed foods in gnotobiotic animals and undernourished children. *Science* **365**, eaau4732 (2019).
34. Hamad, A. F., Alessi-Severini, S., Mahmud, S. M., Brownell, M. & Kuo, I. F. Prenatal antibiotics exposure and the risk of autism spectrum disorders: a population-based cohort study. *PLoS One* **14**, e0221921 (2019).
35. Atladóttir, H. O., Henriksen, T. B., Schendel, D. E. & Parner, E. T. Autism after infection, febrile episodes, and antibiotic use during pregnancy: an exploratory study. *Pediatrics* **130**, e1447–e1454 (2012).

Methods

Mice

C57Bl/6J mice were purchased from Jackson Laboratories, reared as SPF or rederived as GF, and bred in flexible film isolators at the UCLA Center for Health Sciences barrier facility. Animals were maintained on a 12-h light–dark schedule in a temperature-controlled (22–25 °C) and humidity-controlled environment with autoclaved 'breeder' chow (Lab Diets 5K52) and standard chow (Lab Diet 5010) and autoclaved water provided ad libitum.

Sample size determination. Six-to-eight-week-old mice were randomly assigned to experimental groups, which included age- and sex-matched cohorts of males and females for timed matings. Given that maternal microbiome status was the primary experimental variable across experiments, biological sample sizes reflect independent dams. Experiments evaluating fetal outcomes included at least two randomly selected embryos per dam, where data from offspring from a single dam were averaged to represent the dam as the biological *n*. For behavioural assays, all offspring were behaviourally tested and data from offspring from the same dam were averaged to represent the dam as the biological *n*. These data are presented in the main figures, whereas behavioural data per individual offspring are presented in supplementary figures. All experiments were performed in accordance with the NIH Guide for the Care and Use of Laboratory Animals using protocols approved by the Institutional Animal Care and Use Committee at UCLA.

Antibiotic treatment and conventionalization. Four-to-five-week-old SPF mice were gavaged twice daily (08:00 and 17:00) for 1 week with a cocktail of neomycin (100 mg/kg), metronidazole (100 mg/kg), and vancomycin (50 mg/kg), based on methods previously described to mimic GF status[36]. Ampicillin (1 mg/ml) was provided ad libitum in drinking water. Breeders were then paired and time-mated, where up to two additional weeks were required to conception. Gestational day 0.5 was determined by observation of copulation plug. Dams were then separated and maintained on ABX drinking water until E14.5 to avoid the daily stress of oral gavage in pregnant dams (1 mg/ml ampicillin, 1 mg/ml neomycin, and 0.5 mg/ml vancomycin; metronidazole was excluded because of its confounding bitter taste). Faecal samples from ABX-treated dams were collected and plated anaerobically on Schaedler's broth and tryptic soy agar to confirm bacterial clearance. For behavioural assays, pregnant dams were conventionalized at E14.5 with SPF bedding that was gathered from a cage containing male and female C57Bl/6J mice[37]. Pregnant dams were maintained in SPF bedding for the remainder of gestation, and offspring were reared with SPF bedding, added weekly, until behavioural testing. Conventionalization was validated by faecal 16S rRNA gene sequencing and quantitative PCR (qPCR) measurement of 16S rRNA gene loads, as described below. This method of gestational conventionalization of the microbiota restored faecal bacterial loads to SPF levels within 2 days and restored taxonomic diversity of the microbiota to SPF conditions by postnatal day (P)4.

Gnotobiotic colonization. Mice were treated with ABX as described above, then given sterile water and orally gavaged 1 day later with Sp or BD bacteria. Sp-colonized mice were generated as previously described[38]. In brief, faecal pellets from C57Bl/6J SPF mice were freshly suspended in a 10× volume of pre-reduced PBS in an anaerobic chamber. Chloroform was added to 3% (vol/vol) and the sample was shaken vigorously and incubated at 37 °C for 1 h. Chloroform was removed by percolation with CO_2 from a compressed cylinder. Two hundred microlitres of the resultant suspension was orally gavaged into adult GF C57Bl/6J 'founder' mice housed in designated gnotobiotic isolators. Faecal samples were collected from the Sp-colonized mice at more than 2 weeks after gavage and suspended at 50 mg/ml in pre-reduced PBS. Two hundred microlitres of the suspension was orally gavaged to ABX-treated experimental mice. For the *Bacteroides* (BD) consortium, *B. thetaiotaomicron* (ATCC 29148), *B. vulgatus* (ATCC 8482), *B. uniformis* (ATCC 8492), *B. ovatus* (ATCC 8483) and *B. fragilis* (NCTC 9343) were grown in brain heart infusion medium (BD Biosciences) supplemented with 5 μg/ml hemin (Frontier Scientific) and 0.5 μg/ml vitamin K1 (Sigma Aldrich) under anaerobic conditions. A 200-μl suspension of 1:1:1:1:1 OD of each strain was orally gavaged into ABX-treated mice. Colonization status was validated by 16S rRNA gene sequencing of faecal samples collected on E14.5, as described below.

Fetal brain RNA sequencing

Dams were killed on E14.5 by cervical dislocation to preclude the confounding effects of CO_2 on maternal and fetal physiology. Embryonic brains were dissected from the embryos of SPF, ABX, and Sp-colonized mice and placed in Trizol (Invitrogen). RNA was extracted using the RNAeasy Mini kit with on-column genomic DNA-digest (Qiagen), and cDNA synthesis was performed using the qScript cDNA synthesis kit (Quantabio). An RNA integrity number (RIN) of more than 8.0 was confirmed using the 4200 Tapestation system (Agilent). RNA was prepared using the TruSeq RNA Library Prep kit and 2 × 69-bp paired-end sequencing was performed using the Illumina HiSeq 4000 platform by the UCLA Neuroscience Genomics Core. FastQC v0.11.8 and HiSAT2 2.1.0[39,40] were used for quality filtering and mapping. Reads were aligned to UCSC Genome Browser assembly ID: mm10. Differential expression analysis was conducted using DESeq2 1.24.0[41]. Heatmaps were generated using the pheatmap v1.0.12 package for R. GO term enrichment analysis of differentially expressed genes with $q < 0.05$ was conducted using DAVID v6.8[42]. Protein interaction networks were generated using STRING v10.5 with a minimum required interaction score of high confidence (0.700) and maximum number of interactions of no more than 10 interactors. Functional enrichments nodes were categorized by GO: biological process, molecular function, and cellular component and/or KEGG pathways using a false discovery rate (FDR) less than 0.05.

Quantitative RT–PCR

Dams were killed on E14.5 by cervical dislocation to preclude the confounding effects of CO_2 on maternal and fetal physiology. Embryonic brains were dissected and sonicated in Trizol for RNA isolation using the RNAeasy Mini kit with on-column genomic DNA-digest (Qiagen). cDNA synthesis was performed using the qScript cDNA synthesis kit (Quantabio). Quantitative PCR with reverse transcription (qRT–PCR) was performed on a QuantStudio 5 thermocycler (ThermoFisher Scientific) using SYBR green master mix with Rox passive reference dye and validated primer sets obtained from Primerbank (Harvard).

Immunofluorescence staining

E14.5 embryos were fixed in 4% paraformaldehyde for 24 h at 4 °C, cryoprotected in 30% sucrose for 24 h at 4 °C and sectioned at 10 μm using a Leica CM1950 cryostat. Sections were blocked with 10% donkey serum for 1 h. Primary antibodies were diluted in 3% donkey serum and incubated for 15–18 h at 4 °C with netrin-G1a anti-goat antibody (1:100, R&D Systems, AF1166) or neural cell adhesion molecule L1 anti-rat antibody (1:500, EMD Millipore, MAB5272). Sections were then incubated for 2 h at room temperature in their corresponding donkey anti-goat and anti-rat secondary antibodies conjugated to Alexa Fluor 568 or 488 (1:1,000, Thermofisher Scientific). Images were acquired using the Zeiss Axio Examiner LSM 780 confocal microscope with 405 nm (2%), 488 nm (5%), and 561 nm (8%) lasers. Rostral-to-caudal embryonic brain sections were scanned using Zen Blue and Black Edition 2012 software, 20× objective at 1.5× zoom with 5 × 1-μm interval *z*-slices and three individual tracks for each fluorophore. Image acquisition settings included: scan mode set at frame, frame size set at 1024 × 1024, scan speed set at 7, averaging at 2 by line and mean, and bit depth set at 8 bit. Pinhole was set to 1AU.

Image analysis. All images of rostral-to-caudal embryonic brain sections were modified through the same procedures. Images were imported into Fiji, calibrated using a set scale, and adjusted by process > noise > despeckle, to remove non-specific staining, and brightness and contrast settings of 0 minimum and 255 maximum. The whole brain area was measured by manually tracing along the border of each rostral-to-caudal anatomical brain section (0, 200, 400, 600, and 800 µm). To quantify netrin-G1a$^+$ or L1$^+$ integrated density per control ROI, a control ROI was defined as the median area of netrin-G1a staining across SPF control samples for each rostral-to-caudal brain section (Extended Data Fig. 2a). Control ROIs for each rostral to caudal image were saved and superimposed onto corresponding rostral-to-caudal images from all other experimental groups. Integrated density was measured for netrin-G1a, L1, and DAPI staining in each experimental group (SPF, ABX, GF, Sp, BD, ABX + veh, ABX + 4-MM, and ABX + SCFA (short-chain fatty acids)). To address variation in imaging background, netrin-G1a$^+$ or L1$^+$ integrated density was normalized by subtracting the average background integrated density, which was measured from four non-overlapping background ROIs of fixed area that were placed on matched netrinG1a$^-$ cortical and hypothalamic areas in both brain hemispheres of the same section and scaled for size of control ROIs. To normalize netrin-G1a or L1 fluorescence to differences in brain area, a scaling factor was calculated for each image as the mean SPF brain area per rostral-to-caudal image divided by the brain area for corresponding images for each experimental group. Data for netrin-G1a fluorescence intensity were multiplied by this scaling factor for each experimental group per rostral-to-caudal section to generate values normalized for differences in gross brain size. DAPI$^+$ cells were manually counted within matched thalamic areas of the control ROI and similarly normalized to the respective rostral-to-caudal area of brain section. To measure the intensity of netrin-G1a staining, localized areas of netrin-G1a fluorescence were manually traced for each rostral-to-caudal image for each experimental group. The localized areas for each image were used as unique individual ROIs of netrin-G1a$^+$ staining to measure integrated density.

Tissue clearing and imaging

E14.5 embryos were collected and fixed in 4% paraformaldehyde for 48 h at 4 °C. Tissue was rendered transparent using methods for CLARITY-based clearing[43] with the following modifications. Tissues were incubated in a hydrogel solution containing 4% paraformaldehyde, 4% acrylamide (Bio-Rad), 0.05% bis-acrylamide (Bio-Rad), and 0.25% VA-044 (A4P4B0.05) for 3 days at 4 °C. Prior to hydrogel polymerization, the solution was exchanged with new solution lacking bis-acrylamide and paraformaldehyde (A4P04) and polymerized at 37 °C for 3 h. Samples were passively cleared in 8% SDS for 2 weeks at 42 °C, and then incubated with primary antibodies (netrin-G1a anti-goat (1:100, R&D Systems, AF1166) and L1 anti-rat (1:500, EMD Millipore, MAB5272)) for 1 week at 25 °C. Samples were washed and then incubated in secondary antibodies (1:1,000, Thermofisher Scientific) for 5 days at 25 °C. Samples were equilibrated for 15–18 h in a histodenz-based refractive index matching solution (RI 1.47; Sigma Aldrich, D2158) and imaged on a Zeiss LSM 780 with 488 or 561 nm illumination using a 5× objective with 3-µm *z*-slices. Image acquisition settings on the Zen Black 2012 software included: scan mode set at frame, frame size set at 512 × 512, scan speed set to 7, averaging of 2 by line and mean, and bit depth set to 8 bit. Pinhole was set to 1AU.

Images were adjusted for brightness and contrast post hoc with three automated image filter operations in Arivis Vision4D v3.0: 1) denoising to remove noise in the image based on a median filter with a smoothing radius of 2; 2) membrane enhancement to enhance the contrast of dimly labelled axons based on a target membrane width of 0.3 µm and a max gap size of 0.2 µm; and 3) automatic thresholding to segment axonal staining based on an intensity threshold, set by selecting the range of low- to high-intensity pixels mapping to positively stained axonal structures. 3D reconstructions were optically *z*-sliced for manual 3D measurements. Stain volume was quantified using the 'draw objects tool' to segment and interpolate the stained area. The length of axons from the thalamus to the rostral axon tip, circumference of internal capsule and distance from rostral axon tip to cortical surface were measured using the 3D polyline tool to track objects in 2D and measure the entire lengths of objects in 3D. The rostral axon tip was defined as the edge of netrin-G1a staining and cortical surface was defined by the outermost edge of autofluorescence. Positively stained areas of interest were segmented and visualized using CTAn and CTVol software packages (Bruker Corporation), respectively. Netrin-G1a volume (mm^3) was normalized to whole brain volume (mm^3) determined by quantification from microcomputed tomography. Length of axons, circumference of internal capsule, and distance from rostral axon tip to cortical surface (mm) were normalized to the cubic root of whole brain volume (mm).

Microcomputed tomography

Whole embryos were serially dehydrated in ethanol and incubated in 4% (w/v) phosphotungstic acid (EPTA) diluted in 70% EtOH for 4 days at 4 °C. Embryos were scanned at 60 kVp/150 µA with a 1-mm Al filter at a resolution of 8 µm using a benchtop µCT scanner (SkyScan 1275, Bruker). Three-dimensional images were reconstructed following dynamic range adjustment using Gaussian smoothing, a ring artefact reduction of 10, and a defect pixel mask of 8%. Regions of interest (ROI) for brain volume measurements were selected manually, and EPTA-stained tissue was segmented based on contrast to give a final brain volume measurement (mm^3) within the ROI. Whole brain volumes were reconstructed and measured using CTAn and CTVol software (Bruker Corporation).

Axon outgrowth assay

Dams were killed on E14.5 by cervical dislocation to preclude the confounding effects of CO_2 on maternal and fetal physiology. Thalamic, striatal, and hypothalamic explants were isolated from E14.5 embryonic brains and transferred to ice-cold HBSS (Invitrogen). Explants were sliced to ~500 µm and placed on a thin layer of 50-µl BD Matrigel (Beckton Dickinson) on a 15-mm coverslip. Each coverslip contained a thalamic explant at the centre and a striatal and hypothalamic explant on each side, each 1 mm away from the thalamic explant. Explants were incubated in warmed neurobasal complete medium containing 1× neurobasal medium (Thermofisher Scientific), 1× GlutaMax (Thermofisher Scientific), and 2% B-27 (Thermofisher Scientific) for 48 h at 37 °C, and fed with fresh medium every 24 h. After 48 h, the medium was gently aspirated and replaced with 4% PFA for 1 h and processed for immunofluorescence staining with 1:500 β tubulin III anti-mouse antibody (EMD Millipore MAB1637). Axons were imaged using a Leica DMi8 epifluorescence microscope with LasX software and quantified using Fiji software[44]. Images were calibrated using a set scale. Fluorescence images were made binary (grayscale) and 'skeletonized' to visualize axonal arbors. Axon numbers were manually counted per 200 µm of thalamus at a distance of 200 µm from the thalamus. The lengths of the 10 longest axons across a ~500 µm-perimeter proximal to the striatum or the hypothalamus were manually traced from the soma to the furthest distal tip using the Fiji freehand tool. Values were averaged for each explant to report the length of thalamic axons. Data for the number and length of axons in the explant co-culture system were normalized by subtraction of data from monoculture of thalamic explants from the corresponding experimental group.

Metabolite supplementation. Thalamic, striatal, and hypothalamic explants from ABX-treated dams were removed and cultured as described above. For metabolite treatment, BD Matrigel was supplemented with 10 µM, 100 nM, or 1 nM TMAO, 5-AV, IP, 3-IS, or HIP[45–48]. 5-Aminovalerate is a precursor to TMAV, which is not commercially available, and both

have been implicated in carnitine metabolism[49,50]. Metabolite concentrations were determined as physiologically relevant, based on reported concentrations detected in blood and/or cerebrum from the mouse multiple tissue metabolomic database (MMMDB), human metabolome database (HMDB) and existing literature[45–48]. Axons were stained, imaged and analysed as described above. There were no overt differences in the pH of metabolite solutions.

In vivo metabolite supplementation

To test the effects of TMAO, 5-AV, IP, and HIP on fetal axonogenesis and behaviour, physiological concentrations of metabolites were administered intraperitoneally as a single dose per day in order to limit stress to pregnant dams. Control dams were injected with vehicle. Metabolite dosages were calculated on the basis of maternal serum metabolomic data and physiological concentrations reported in the literature to reflect daily levels needed to achieve those observed in SPF dams. Metabolite concentrations were calculated using physiological levels reported in mouse blood[45–48], total blood volume of pregnant mouse dams (approximately 58.5 ml/kg[51]), and relative reductions observed in maternal sera of ABX dams compared to SPF dams (Supplementary Tables 6, 7). The metabolite mixture (4-MM: 121 μg TMAO, 9 μg 5-AV, 92 μg IP, and 2 μg HIP in 200 μl of 0.1 M PBS) was injected intraperitoneally into E7.5 ABX dams once a day for 7 days. To assess fetal thalamocortical axon levels, dams treated with 4-MM or vehicle were killed on E14.5, and fetal brains were removed and processed as described in 'Immunofluorescence staining' above. To test for behavioural effects, E14.5 pregnant dams were taken off ABX water (ANV) on E14.5, transferred into cages with sterile water, and conventionalized as described in 'Antibiotic treatment and conventionalization' above. Adult offspring (P42–P56) were tested using the von Frey filament test and adhesive removal test as described below.

To test whether SCFAs affect embryonic axon development, the SCFAs sodium propionate (25 mM), sodium butyrate (40 mM), and sodium acetate (67.5 mM) were added to the drinking water of pregnant ABX dams from E0 to E14.5, following reported physiological concentrations[52]. Supplemented drinking water was sterile-filtered and made freshly every 4 days. ABX dams supplemented with SCFA were killed at E14.5 and embryonic brains were isolated and processed for immunofluorescence staining as described above.

Behavioural assays

For behavioural assays, investigators were blinded to experimental groups. Animals were tested in behavioural assays between 6 and 10 weeks of age, progressing from the least to the most stress-inducing behavioural task, in the order listed below. To prevent stress as a confounding factor, there was a 2–3-day break between behavioural assays. For each behavioural test, cages were brought to the testing room at least 30 min before testing to enable acclimation and reduce stress. Equipment and testing chambers were thoroughly cleaned with Accel disinfectant (Unimed) before and after each trial.

Visual cliff avoidance test. To assess depth perception and visual impairment[3], mice were placed in a 42.5 cm × 60 cm clear plexiglass testing chamber on top of a 3 ft × 4 ft rectangular table. One third of the chamber hung over the edge of the table to create the visual effect of a cliff drop-off at a height of 3 ft. Mice were placed in the middle of the chamber ten times. Mice were given 5 min to exit the middle third of the chamber towards the third of the chamber that is over the table or towards the third of the chamber that is the cliff side. Choices were recorded and averaged by an experimenter blinded to mouse experimental group.

Novel whisker texture test. The whisker texture test was performed using methods adapted from Wu et al.[2]. Mice were habituated in 50 cm × 50 cm white plexiglass testing chamber for 10 min for 2 consecutive days. On testing day, mice were first subjected to a learning phase in which they were placed in the testing chamber for 5 min with two objects of identical texture (aluminium oxide sand paper, 80 grit). Mice were then returned to the home cage for 5 min. In the test phase, mice were placed back into the chamber with two objects, one with the original texture (80 grit) and one with a new texture (220 grit). The trials were recorded with an overhead video camera and Ethovision XT v11.5 software (Noldus) was used to analyse the number of times and duration spent investigating the novel and familiar textures.

Adhesive removal test. The adhesive removal test was performed according to methods adapted from Bouet et al.[15]. In brief, mice were acclimated to the testing cage for 5 min. A small adhesive tape (0.3 cm × 0.4 cm) was gently applied to both forepaws, and mice were returned to the testing cage. Mice were observed for contact time, defined as the latency to the mouse's first reaction to the presence of the adhesive tape, and for removal time, defined as the latency to complete removal of both pieces of tape by the mouse. Contact time and removal time were manually recorded using a standard lab multi-timer by experimenters blinded to the mouse experimental group.

von Frey filament test. The von Frey filament test was performed according to methods adapted from Dixon et al.[53]. In brief, mice were placed on a wide gauge, wire mesh surface in a testing chamber and acclimated for 10 min daily for two consecutive days before testing day. On the testing day, mice were placed in the testing chamber and acclimated for 10 min before von Frey filaments were applied from the underside of the mesh to the plantar surface of the hindpaw. The process was repeated with increasing gauges (0.4, 0.6, 1, 1.4, 2, 4, 6 g of force) of von Frey filaments until stimulation elicited hindpaw withdrawal, wherein the mouse responds by flicking its paw away from the stimulus. Upon paw withdrawal, the next weaker stimulus was defined as threshold. Responses to up–down paw stimulation were manually recorded and analysed according to the Chaplan Method of 50% paw withdrawal threshold[14].

Hot-plate test. To test for somatic pain responses[1], mice were acclimated to a clear plastic cylinder for 30 s, then placed on an advanced hot plate (VWR) that was heated to 52 °C. The latency to show a nociceptive response (a paw lick, paw flick, vocalization, or jump) was recorded, and the mouse was immediately returned to the home cage.

Rotarod test. To test for motor coordination and balance[4], mice were placed in one of four compartments in a rotarod apparatus (Rotamex, Columbus Instruments) consisting of a cylinder that rotates at speeds that accelerate from 5 rpm to 60 rpm in 300 s. On the first day, mice acclimated to the apparatus with no rotation for 2 min. On the testing day, mice were returned to the apparatus and rotation was initiated. Latency to fall and final speed achieved by the accelerating rod before falling were detected using an infrared sensor and recorded. Mice were tested three times and scores were averaged.

Prepulse inhibition test. The prepulse inhibition test was performed to measure sensorimotor gating[54]. Mice were placed in a restraint tube mounted on a startle measuring platform (San Diego Instruments) and acclimated to the testing chamber for 10 min. White noise was presented in the recording chamber for 5 min, followed by 6 startle presentations and a pseudorandomized prepulse inhibition phase, which consisted of either no startle, 120 db startle stimulus only, or 70 db prepulse with startle, 75 db prepulse with startle, or 80 db prepulse with startle. Acoustic startle was recorded with a piezo-electric sensor, and the percentage prepulse inhibition was defined as: (((startle stimulus only − prepulse with startle)/startle stimulus only) × 100).

16S rRNA gene sequencing

Bacterial genomic DNA was extracted from mouse faecal samples using the MoBio PowerSoil Kit (now DNeasy PowerSoil Kit, Qiagen). Quantification of 16S rRNA gene loads was performed by qPCR using the SYBR Green master mix (Thermo Fisher), universal 16S rRNA gene primers[55] and the QuantStudio 5 thermocycler (cycling parameters: 2 min at 50 °C, 10 min at 95 °C, 40 cycles of 10 s at 95 °C, and 45 s at 62 °C). Sequencing libraries were generated using methods adapted from Caporaso et al.[56]. The V4 regions of the 16S rRNA gene were PCR amplified using individually barcoded universal primers and 30 ng of the extracted genomic DNA. The PCR reaction was set up in triplicate, and the PCR product was purified using the Qiaquick PCR purification kit (Qiagen). Two hundred and fifty nanograms of purified PCR product from each sample was pooled and sequenced by Laragen, Inc. using the Illumina MiSeq platform and 2 × 250 bp reagent kit for paired-end sequencing. Deblur was used for quality control[57] and operational taxonomic units (OTUs) were chosen on the basis of 99% sequence similarity to SILVA 132. Taxonomy assignment and rarefaction were performed using QIIME2[58]. OTUs were ordered by relative abundance with phyloseq[59] and taxa bar plots were generated using Fantaxtic R package.

Metabolomics

At E14.5, maternal serum was collected by cardiac puncture, separated using SST vacutainer tubes (Beckton Dickinson) and frozen at −80 °C. Embryonic brains were removed and immediately snap frozen in liquid nitrogen. Each fetal brain sample consisted of five embryonic brains pooled from the same litter. Samples were prepared using the automated MicroLab STAR system (Hamilton Company) and analysed on gas chromatography (GC)–mass spectrometry (MS), liquid chromatography (LC)–MS and LC–MS/MS platforms by Metabolon, Inc. Protein fractions were removed by serial extraction with organic aqueous solvents, concentrated using a TurboVap system (Zymark) and vacuum dried. For LC–MS and LC–MS/MS, samples were reconstituted in acidic or basic LC-compatible solvents containing >11 injection standards and run on a Waters ACQUITY UPLC and Thermo-Finnigan LTQ mass spectrometer, with a linear ion-trap frontend and a Fourier transform ion cyclotron resonance mass spectrometer back-end. For GC–MS, samples were derivatized under dried nitrogen using bistrimethyl-silyl-trifluoroacetamide and analysed on a Thermo-Finnigan Trace DSQ fast-scanning single-quadrupole mass spectrometer using electron impact ionization. Chemical entities were identified by comparison to metabolomic library entries of purified standards. Following log transformation and imputation with minimum observed values for each compound, data were analysed using one-way ANOVA to test for group effects. P and q values were calculated using two-way ANOVA contrasts. Principal components analysis was used to visualize variance distributions. Volcano plots were generated using R, with differentially regulated metabolites at $q < 0.05$. Supervised random forest analysis was conducted to identify metabolomic prediction accuracies based on a group of decision trees[60]. In brief, randomly selected data from samples across all microbiota conditions were used to build trees. Remaining data were then passed down the trees to generate class prediction values of microbiota status for each sample. This process was performed thousands of times to generate the forest, and each sample's microbiota status was determined by computing the class prediction frequency of the remaining variables over the whole forest. Class predictions of microbiota status were then compared to true microbiota status for each sample, and this error rate served as a measure of prediction accuracy. The metabolites that contributed the most to the microbiota status classification were determined using the mean decrease accuracy metric, or by randomly permuting a metabolite, running the observed values through the trees and reassessing the microbiota status prediction accuracy.

Statistics and reproducibility

Statistical analysis was performed using Prism software (GraphPad v6). All statistical results are included as Supplementary Table 8. Data were assessed for normal distribution and plotted in the figures as mean ± s.e.m. For each figure, n = the number of independent maternal biological replicates. For assessments involving fetal brains, each maternal biological sample reflects an average of 2–5 embryo 'technical' replicates. For behavioural assessments, all offspring were tested. Data for littermates from the same dam were averaged and presented in the main figures with n denoting independent maternal dams; individual data for each offspring are provided in Extended Data Fig. 6. No samples or animals were excluded from the analyses. Quantitative RT–PCR, immunofluorescence staining, axon outgrowth assay, and behavioural experiments were replicated at least three times with similar results. Differences among more than two groups with only one variable were assessed using one-way ANOVA with Tukey's or Sidak's post hoc test. Taxonomic comparisons from 16S rRNA gene sequencing analysis were analysed using the Kruskal–Wallis test with Tukey's post hoc test. Two-way ANOVA with Tukey's or Sidak's post hoc test was used for comparisons of two or more groups with two variables. Significant differences emerging from the above tests are indicated in the figures by $^{*}P < 0.05$, $^{**}P < 0.01$, $^{***}P < 0.001$, $^{****}P < 0.0001$. Notable non-significant differences are indicated in the figures by NS.

Reporting summary

Further information on research design is available in the Nature Research Reporting Summary linked to this paper.

Data availability

All data generated and analysed during this study are included in this published article and its Supplementary Information files. The 16S rRNA gene sequencing data that support the findings have also been deposited to the Qiita database (https://qiita.ucsd.edu/) with study IDs 13099, 13106 and 13107. Transcriptomic data that support the findings of this study have also been deposited to the Gene Expression Omnibus (GEO) repository with accession number GSE147183. Source data are provided with this paper.

36. Reikvam, D. H. et al. Depletion of murine intestinal microbiota: effects on gut mucosa and epithelial gene expression. *PLoS One* **6**, e17996 (2011).
37. McVey Neufeld, K. A., Perez-Burgos, A., Mao, Y. K., Bienenstock, J. & Kunze, W. A. The gut microbiome restores intrinsic and extrinsic nerve function in germ-free mice accompanied by changes in calbindin. *Neurogastroenterol. Motil.* **27**, 627–636 (2015).
38. Yano, J. M. et al. Indigenous bacteria from the gut microbiota regulate host serotonin biosynthesis. *Cell* **161**, 264–276 (2015).
39. Kim, D., Langmead, B. & Salzberg, S. L. HISAT: a fast spliced aligner with low memory requirements. *Nat. Methods* **12**, 357–360 (2015).
40. Pertea, M., Kim, D., Pertea, G. M., Leek, J. T. & Salzberg, S. L. Transcript-level expression analysis of RNA-seq experiments with HISAT, StringTie and Ballgown. *Nat. Protocols* **11**, 1650–1667 (2016).
41. Love, M. I., Huber, W. & Anders, S. Moderated estimation of fold change and dispersion for RNA-seq data with DESeq2. *Genome Biol.* **15**, 550 (2014).
42. Huang, W., Sherman, B. T. & Lempicki, R. A. Systematic and integrative analysis of large gene lists using DAVID bioinformatics resources. *Nat. Protocols* **4**, 44–57 (2009).
43. Chung, K. et al. Structural and molecular interrogation of intact biological systems. *Nature* **497**, 332–337 (2013).
44. Schindelin, J. et al. Fiji: an open-source platform for biological-image analysis. *Nat. Methods* **9**, 676–682 (2012).
45. Koh, A. et al. Microbially produced imidazole propionate impairs insulin signaling through mTORC1. *Cell* **175**, 947–961 (2018).
46. Mishima, E. et al. Evaluation of the impact of gut microbiota on uremic solute accumulation by a CE-TOFMS-based metabolomics approach. *Kidney Int.* **92**, 634–645 (2017).
47. Soga, T. et al. Differential metabolomics reveals ophthalmic acid as an oxidative stress biomarker indicating hepatic glutathione consumption. *J. Biol. Chem.* **281**, 16768–16776 (2006).
48. Soga, T. et al. Quantitative metabolome analysis using capillary electrophoresis mass spectrometry. *J. Proteome Res.* **2**, 488–494 (2003).
49. Kärkkäinen, O. et al. Whole grain intake associated molecule 5-aminovaleric acid betaine decreases β-oxidation of fatty acids in mouse cardiomyocytes. *Sci. Rep.* **8**, 13036 (2018).

50. Fothergill, J. C. & Guest, J. R. Catabolism of L-lysine by *Pseudomonas aeruginosa*. *J. Gen. Microbiol*. **99**, 139–155 (1977).
51. Diehl, K. H. et al. A good practice guide to the administration of substances and removal of blood, including routes and volumes. *J. Appl. Toxicol*. **21**, 15–23 (2001).
52. Erny, D. et al. Host microbiota constantly control maturation and function of microglia in the CNS. *Nat. Neurosci*. **18**, 965–977 (2015).
53. Deuis, J. R., Dvorakova, L. S. & Vetter, I. Methods used to evaluate pain behaviors in rodents. *Front. Mol. Neurosci*. **10**, 284 (2017).
54. Perry, W., Minassian, A., Lopez, B., Maron, L. & Lincoln, A. Sensorimotor gating deficits in adults with autism. *Biol. Psychiatry* **61**, 482–486 (2007).
55. Barman, M. et al. Enteric salmonellosis disrupts the microbial ecology of the murine gastrointestinal tract. *Infect. Immun*. **76**, 907–915 (2008).
56. Caporaso, J. G. et al. Global patterns of 16S rRNA diversity at a depth of millions of sequences per sample. *Proc. Natl Acad. Sci. USA* **108** (Suppl. 1), 4516–4522 (2011).
57. Amir, A. et al. Deblur rapidly resolves single-nucleotide community sequence patterns. *mSystems* **2**, e00191-16 (2017).
58. Bolyen, E. et al. Reproducible, interactive, scalable and extensible microbiome data science using QIIME 2. *Nat. Biotechnol*. **37**, 852–857 (2019).
59. McMurdie, P. J. & Holmes, S. phyloseq: an R package for reproducible interactive analysis and graphics of microbiome census data. *PLoS One* **8**, e61217 (2013).
60. Breiman, L. Random forests. *Mach. Learn*. **45**, 5–32 (2001).

Acknowledgements We thank members of the Hsiao lab for their critical review of the manuscript; T. Su for RNA sequencing advice; A. Oyler-Yaniv, J. Oyler-Yaniv and R. Wollman for assistance with initial light-sheet image acquisition; A. Rajbhandari and Irina Zhuravka of the UCLA Behavioral Testing Core for behavioural assay training; S. White for sharing ultrasonic vocalization equipment; and A. Collazo of the Caltech Beckman Institute Biological Imaging Facility for assistance with light-sheet image acquisition and analysis. Support for this research was provided by the Packard Fellowship in Science and Engineering and Klingenstein-Simons Award to E.Y.H.; UPLIFT: UCLA Postdocs' Longitudinal Investment in Faculty Award (# K12 GM106996) and NICHD Pathway to Independence Award (#K99 HD101680) to H.E.V.; the Ruth L. Kirschstein National Research Service Awards (#F31 HD101270 to G.N.P. and #F30 DE025172 to D.W.W.), and the NSF Graduate Research Fellowship to E.J.L.C. E.Y.H. is a New York Stem Cell Foundation – Robertson Investigator. This research was supported in part by the New York Stem Cell Foundation.

Author contributions H.E.V. led and performed all experiments; G.N.P. assisted with sample collection and data analysis for imaging, 16S rRNA gene sequencing and metabolomic experiments; D.W.W. assisted with CLARITY, microcomputed tomography and imaging experiments; E.J.L.C., E.L.S., A.Q., M.K. and C.J.W. assisted with axon outgrowth, behavioural, immunofluorescence staining and/or imaging experiments; T.R. generated gnotobiotic mice; E.Y.H. supervised the study; and H.E.V., G.N.P. and E.Y.H. wrote the manuscript.

Competing interests Findings regarding the manipulation of the maternal microbiome to influence fetal development and sensory behavior reported in the manuscript are the subject of provisional patent application US 62/844,503, owned by UCLA. The authors declare no competing interests.

Additional information

Supplementary information is available for this paper at https://doi.org/10.1038/s41586-020-2745-3.

Correspondence and requests for materials should be addressed to H.E.V.

Peer review information *Nature* thanks Tianyi Mao and the other, anonymous, reviewer(s) for their contribution to the peer review of this work.

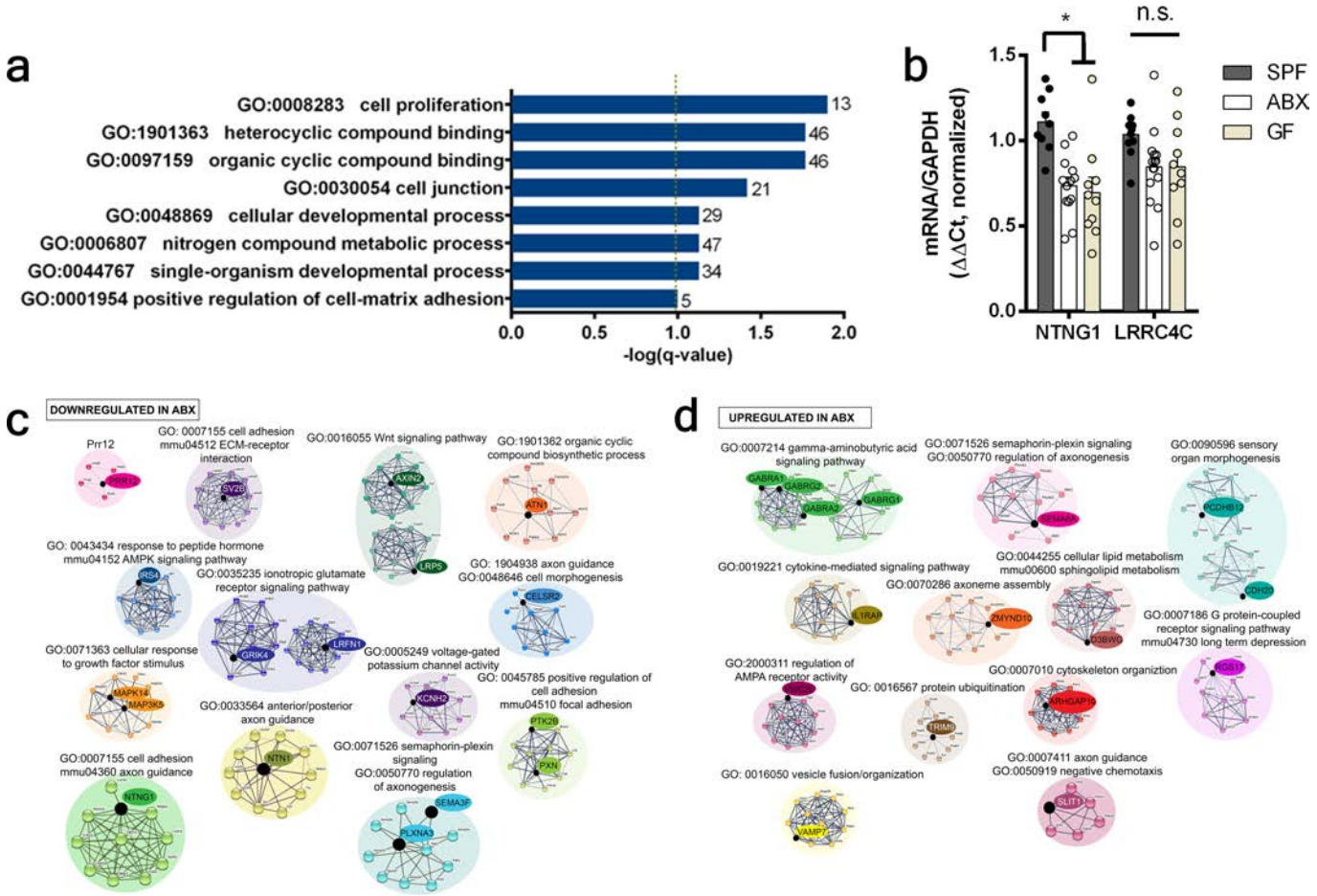

Extended Data Fig. 1 | Network analysis and qPCR validation of fetal brain RNA-seq data. a, Gene ontology analysis of differentially expressed genes from E14.5 brains from ABX versus SPF dams (one-tailed Fisher exact, $q = 0.0125, 0.017, 0.017, 0.0383, 0.0745, 0.0745, 0.0745, 0.1002$, $n = 3$ dams). **b**, Quantitative RT–PCR for *Ntng1* and *LRRC4C* expression in E14.5 brains from offspring of SPF, ABX or GF dams (two-way ANOVA+Tukey's, $n = 9, 15, 10$ dams). **c**, Protein interaction network of genes downregulated in E14.5 brains from offspring of ABX vs. SPF dams (Benjamini-Hochberg, $q < 0.05$, $n = 3$ dams). **d**, Protein interaction networks of genes upregulated in E14.5 brains from offspring of ABX vs. SPF dams (Benjamini-Hochberg, $q < 0.05$, $n = 3$ dams). Mean ± SEM. $^*P < 0.05$, n.s. = not statistically significant.

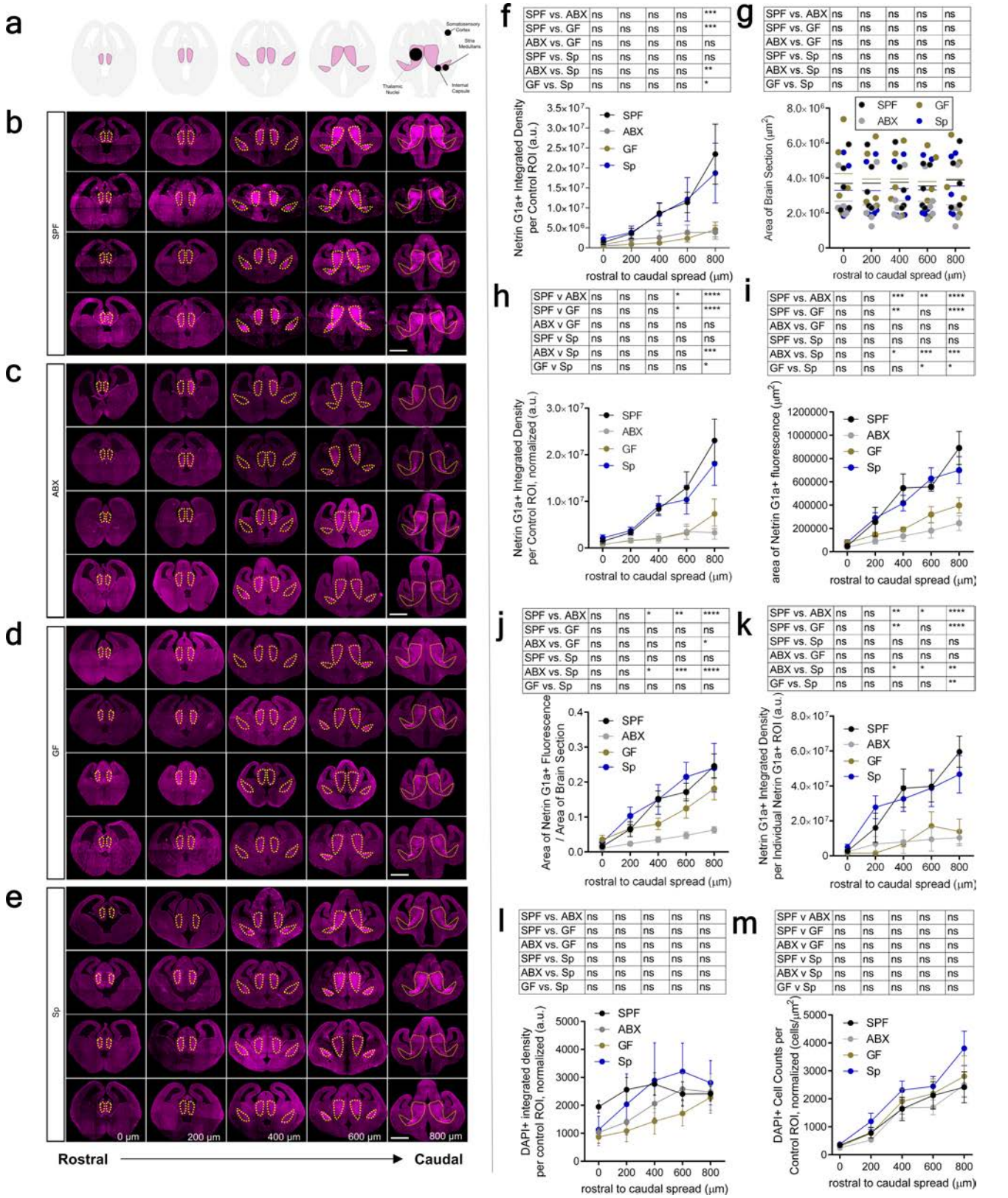

Extended Data Fig. 2 | See next page for caption.

Extended Data Fig. 2 | Netrin-G1a thalamocortical axons in E14.5 brains of offspring from gnotobiotic dams. a, Reference diagrams of coronal rostral to caudal E14.5 brain sections. **b**–**e**, Netrin-G1a in four independent E14.5 brains from offspring of SPF (**b**), ABX (**c**), GF (**d**), and Sp (**e**) dams. Scale = 500 µm. Yellow lines = matched control ROI. **f**, Netrin-G1a fluorescence per control ROI in E14.5 brain sections of offspring from SPF, ABX, GF and Sp dams. SPF, ABX, GF and Sp data are as presented in Fig. 1c and 2d. (Two-way ANOVA+Tukey's, $n = 5$ dams). **g**, Total brain area E14.5 brain section of offspring from SPF, ABX, GF and Sp dams. (Two-way ANOVA+Tukey's, $n = 5$ dams). **h**, Netrin-G1a per matched control ROI, normalized by total brain area in E14.5 brain sections of offspring from SPF, ABX, GF and Sp dams. (Two-way ANOVA+Tukey's, $n = 5$ dams). **i**, Area of Netrin-G1a in E14.5 brain sections of SPF, ABX, GF and Sp dams. (Two-way ANOVA+Tukey's, $n = 5$ dams). **j**, Area of Netrin-G1a+ staining normalized by total brain area in E14.5 brain sections of offspring from SPF, ABX, GF and Sp dams. (Two-way ANOVA+ Tukey's, $n = 5$ dams). **k**, Netrin-G1a fluorescence in area of Netrin-G1a+ staining of E14.5 brains from SPF, ABX, GF, and Sp dams. (Two-way ANOVA+Tukey's, $n = 5$ dams). **l**, DAPI per matched control ROI, normalized by total brain area in E14.5 brain sections from SPF, ABX, GF and Sp dams. (Two-way ANOVA+Tukey's, $n = 5, 7, 4, 5$ dams). **m**, DAPI+ cell per matched control ROI, normalized by total brain area in E14.5 brain sections from SPF, ABX, GF and Sp dams. (Two-way ANOVA+ Tukey's, $n = 5, 7, 4, 5$ dams). Mean ± SEM. $^{*}P < 0.05$, $^{**}P < 0.01$, $^{***}P < 0.001$, $^{****}P < 0.0001$, n.s. = not statistically significant.

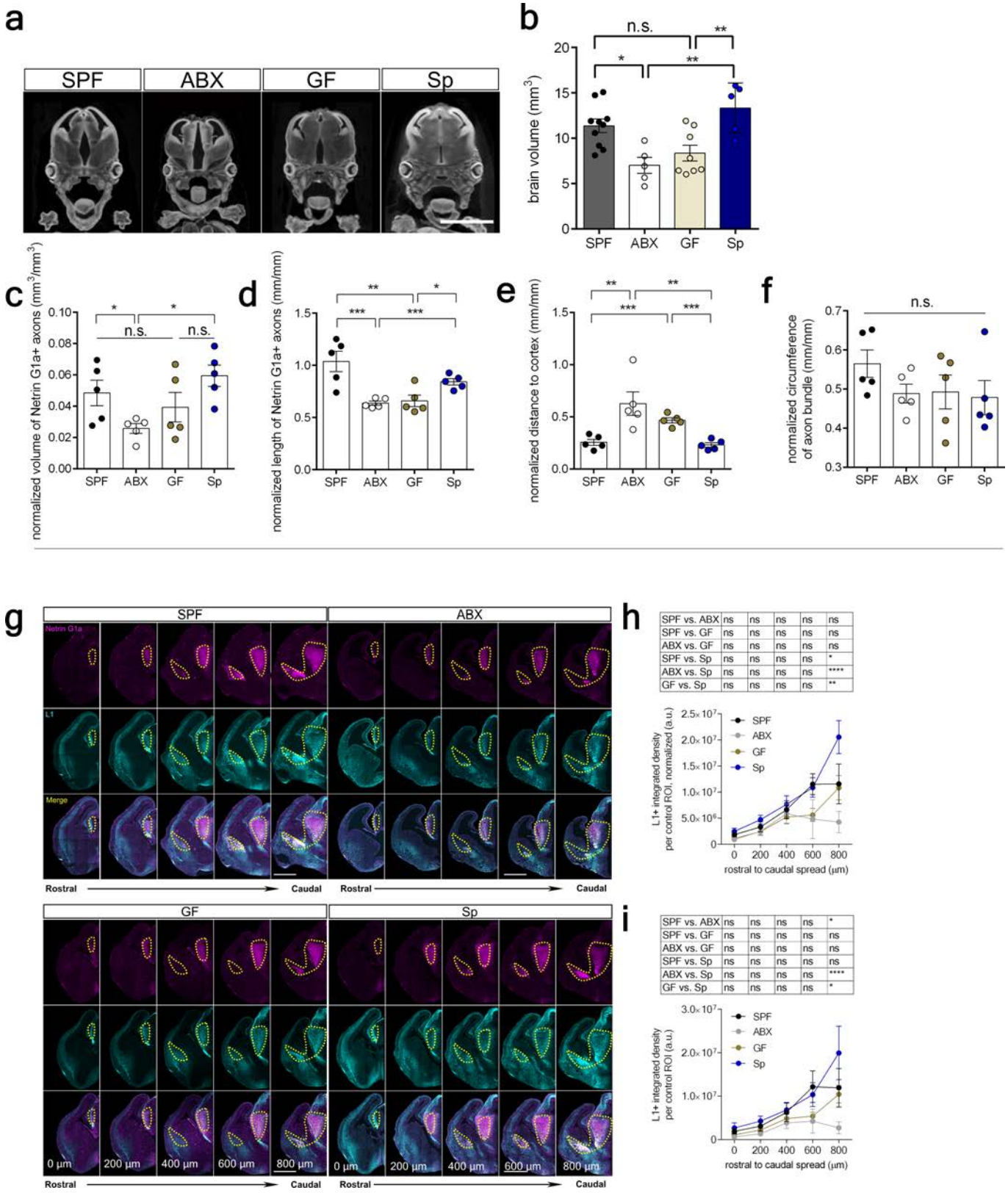

Extended Data Fig. 3 | See next page for caption.

Extended Data Fig. 3 | Whole brain volume and L1$^+$ thalamocortical axons in E14.5 brains of offspring from gnotobiotic dams. a, Micro-computed tomography of E14.5 fetal brain. Scale bar = 2 mm. **b**, Whole fetal brain volume of E14.5 offspring from SPF, ABX, GF and Sp dams. (One-way ANOVA+Tukey's, $n = 10, 5, 8, 5$ dams). **c**, Volume of Netrin-G1a axons, normalized to E14.5 SPF, ABX, GF, and Sp whole brain volume. (SPF v ABX: two-tailed Mann–Whitney, SPF v GF, GF v Sp, and ABX v Sp: One-way ANOVA+Tukey's, $n = 5$ offspring from different dams). **d**, Length of Netrin-G1a axons, normalized to the cubic root of E14.5 SPF, ABX, GF, and Sp whole brain volume. (SPF v ABX and SPF v GF: One-way ANOVA+Tukey's, Sp v ABX and Sp v GF: two-tailed Mann–Whitney, $n = 5$ offspring from different dams). **e**, Distance from rostral tip of Netrin-G1a axon to cortex, normalized to the cubic root of E14.5 SPF, ABX, GF, and Sp whole brain volume. (SPF v ABX and Sp v ABX: One-way ANOVA+Tukey's, SPF v GF and Sp v GF: two-tailed Mann–Whitney, $n = 5$ offspring from different dams). **f**, Circumference of Netrin-G1a axonal bundle at the internal capsule (IC), normalized to the cubic root of E14.5 SPF, ABX, GF, and Sp whole brain volume. (One-way ANOVA+Tukey's, $n = 5$ offspring from different dams). **g**, Netrin-G1a (magenta) and L1 (cyan) in E14.5 SPF, ABX, GF and Sp brain sections. Scale = 500 µm. Yellow lines = matched control ROI. **h**, L1 per matched control ROI, normalized by total brain area in E14.5 SPF, ABX, GF and Sp brain sections. (Two-way ANOVA+Tukey's, $n = 5$ dams). **i**, L1 per matched control ROI in E14.5 brain sections of offspring from SPF, ABX, GF and Sp dams. SPF, ABX, GF, and Sp data are as in Fig. 1d and 2e. (Two-way ANOVA+Tukey's, $n = 5$ dams). Mean ± SEM, $^*P < 0.05$, $^{**}P < 0.01$, $^{****}P < 0.0001$, n.s. = not statistically significant.

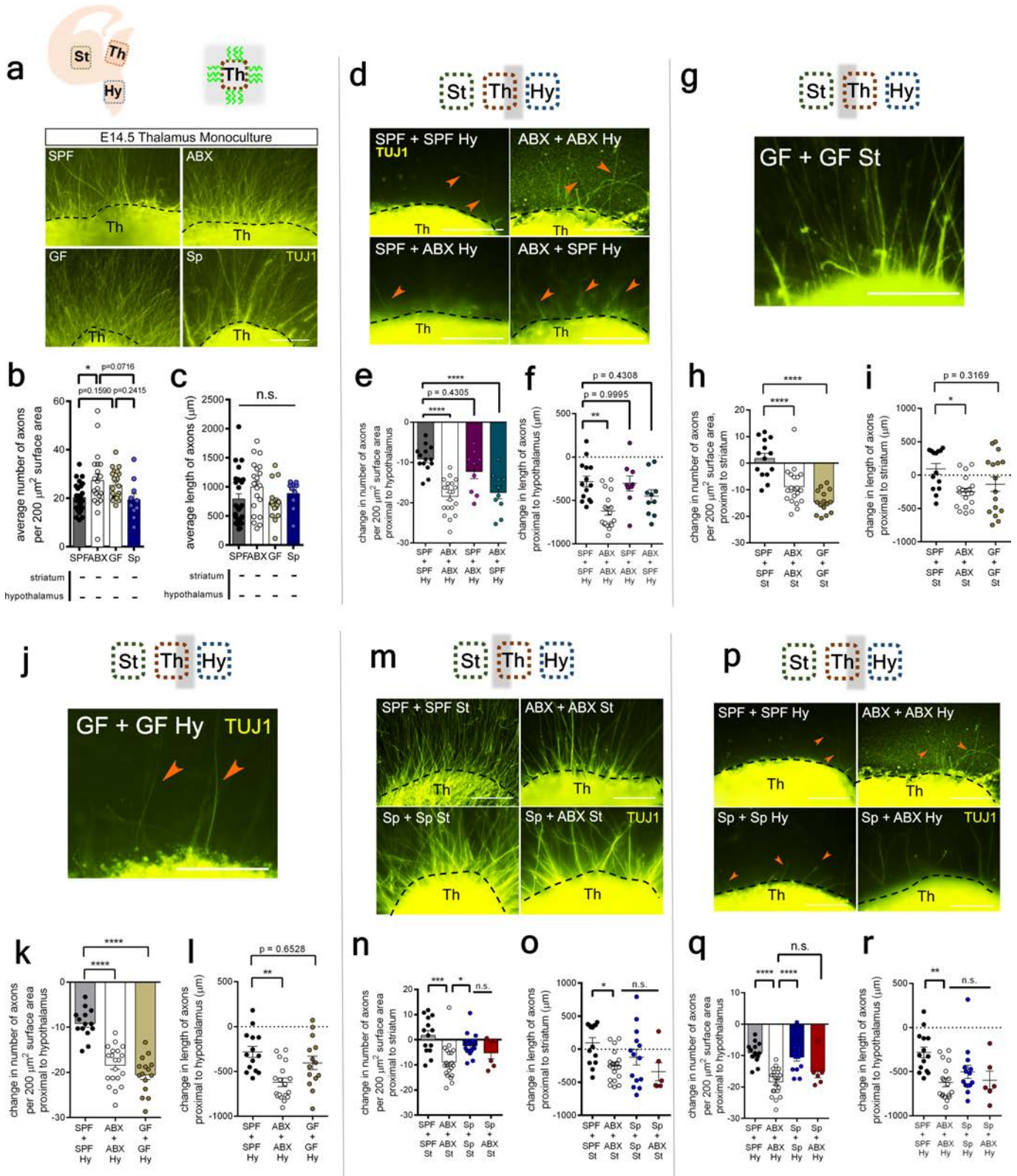

Extended Data Fig. 4 | See next page for caption.

Extended Data Fig. 4 | Thalamic explant monocultures and co-cultures with striatal and hypothalamic explants. a, Axon outgrowth from monoculture of thalamic explants (Th) from E14.5 offspring of SPF, ABX, GF and Sp dams. Scale = 250 µm. In Th monocultures: **b**, axon number, and **c**, axon length (One-way ANOVA+Tukey's, $n = 26, 20, 21, 10$ explants). **d**, Axon outgrowth from (i) SPF Th+SPF hypothalamic explant (Hy), (ii) ABX Th+ABX Hy, (iii) SPF Th+ABX Hy, (iv) ABX Th+SPF Hy. Scale = 250 µm. Proximal to Hy: **e**, axon number /200 µm^2 surface area, normalized to Th monoculture, and **f**, axon length, normalized to Th monoculture. (One-way ANOVA+Tukey's, $n = 14, 20, 9, 10$ explants). **g**, Axon outgrowth from GF Th+GF St. Scale bar = 250 µm. Proximal to St: **h**, axon number/200 µm^2 surface area, normalized to Th monoculture, and **i**, axon length, normalized to Th monoculture. (One-way ANOVA+Tukey's, $n = 16$ GF explants). **j**, Axon outgrowth from GF Th+GF Hy. Scale bar = 250 µm. Proximal to Hy: **k**, axon number/200 µm^2 surface area, normalized to Th monoculture, and **l**, axon length, normalized to Th monoculture. (One-way ANOVA+Tukey's, $n = 14$ GF explants). **m**, Axon outgrowth from (i) SPF Th+SPF St, (ii) ABX Th+ABX St, (iii) Sp Th+Sp St, (iv) Sp Th+ABX St. Scale = 250 µm. Proximal to St: **n**, axon number/200 µm^2 surface area, normalized to Th monoculture, and **o**, axon length, normalized to Th monoculture. (One-way ANOVA+Tukey's, $n = 14, 20, 14, 6$ explants.) **p**, Axon outgrowth from (i) SPF Th+SPF Hy, (ii) ABX Th+ABX Hy, (iii) Sp Th+Sp Hy, (iv) Sp Th+ABX Hy. Arrows = sparse short axons. Scale = 250 µm. Proximal to Hy: **q**, axon number/200 µm perimeter, normalized to Th monoculture, and **r**, axon length, normalized to Th monoculture. (One-way ANOVA+Tukey's, $n = 14, 20, 14, 6$ explants). SPF and ABX data in g-i and m-o are in Fig. 1k, 1l. Mean ± SEM. $^*P < 0.05$, $^{**}P < 0.01$, $^{***}P < 0.001$, $^{****}P < 0.0001$, n.s. = not statistically significant.

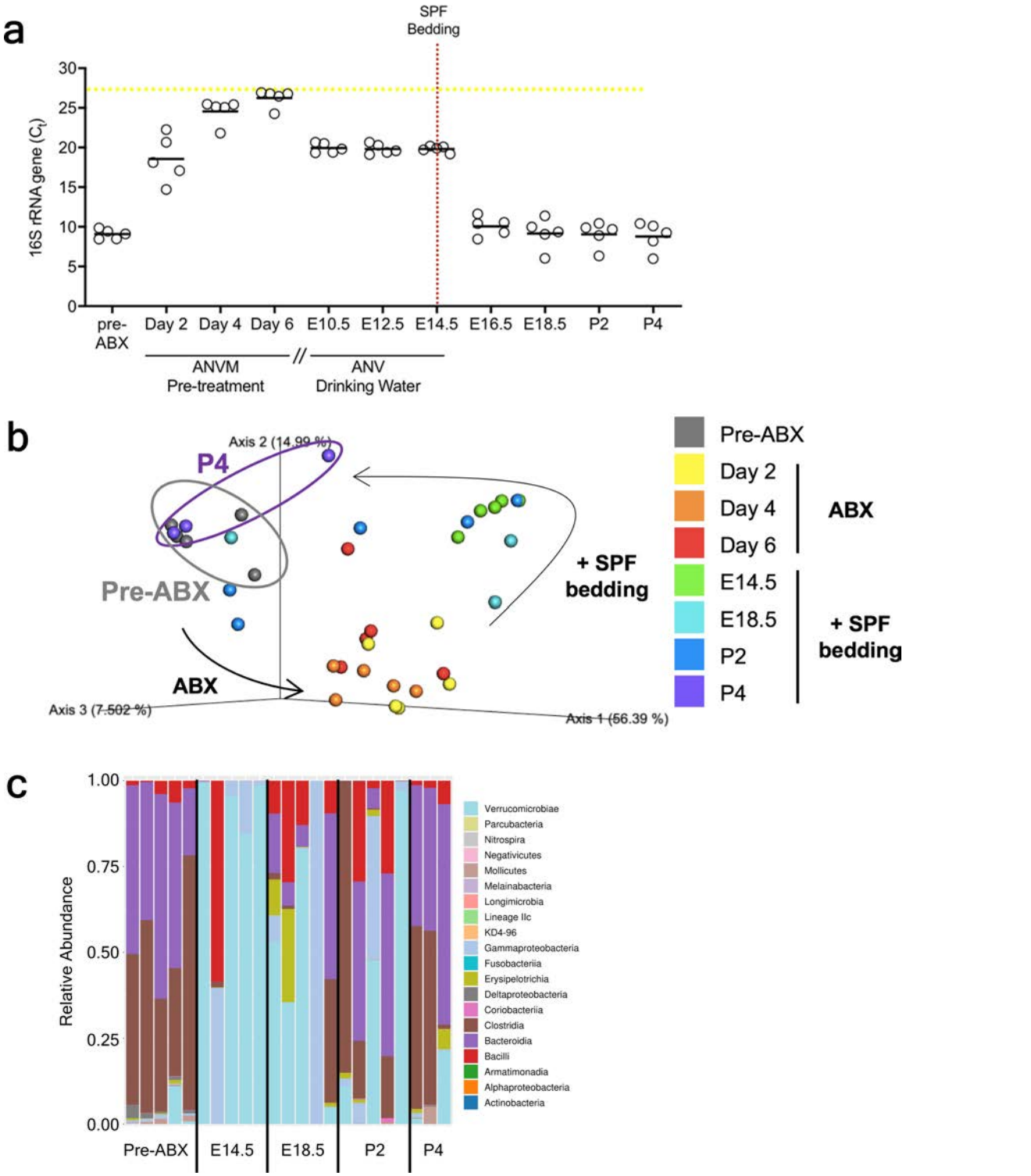

Extended Data Fig. 5 | Effects of maternal antibiotic treatment and gestational conventionalization on the faecal microbiota. a, Bacterial load of the maternal faecal microbiota in response to antibiotic (ANVM = ampicillin, neomycin, vancomycin, metronidazole) treatment and conventionalization with SPF microbiota. Yellow line = Ct of germ-free control. (n = 5 cages). **b**, Principal coordinate analysis of 16S rRNA gene sequencing data (weighted Unifrac distances) for maternal faecal microbiota before antibiotic treatment (pre-ABX), on Day 2, 4, or 6 after ABX treatment, and on Day 0 (E14.5), 4 (E18.5), 6 (P2) and 8 (P4) after exposure to SPF bedding. (n = 5, 5, 5, 5, 3 cages). **c**, Class-level taxonomic diversity of maternal faecal microbiota pre-ABX and on Day 0 (E14.5), 4 (E18.5), 6 (P2) and 8 (P4) after exposure to SPF bedding. (n = 5, 5, 5, 5, 3 cages).

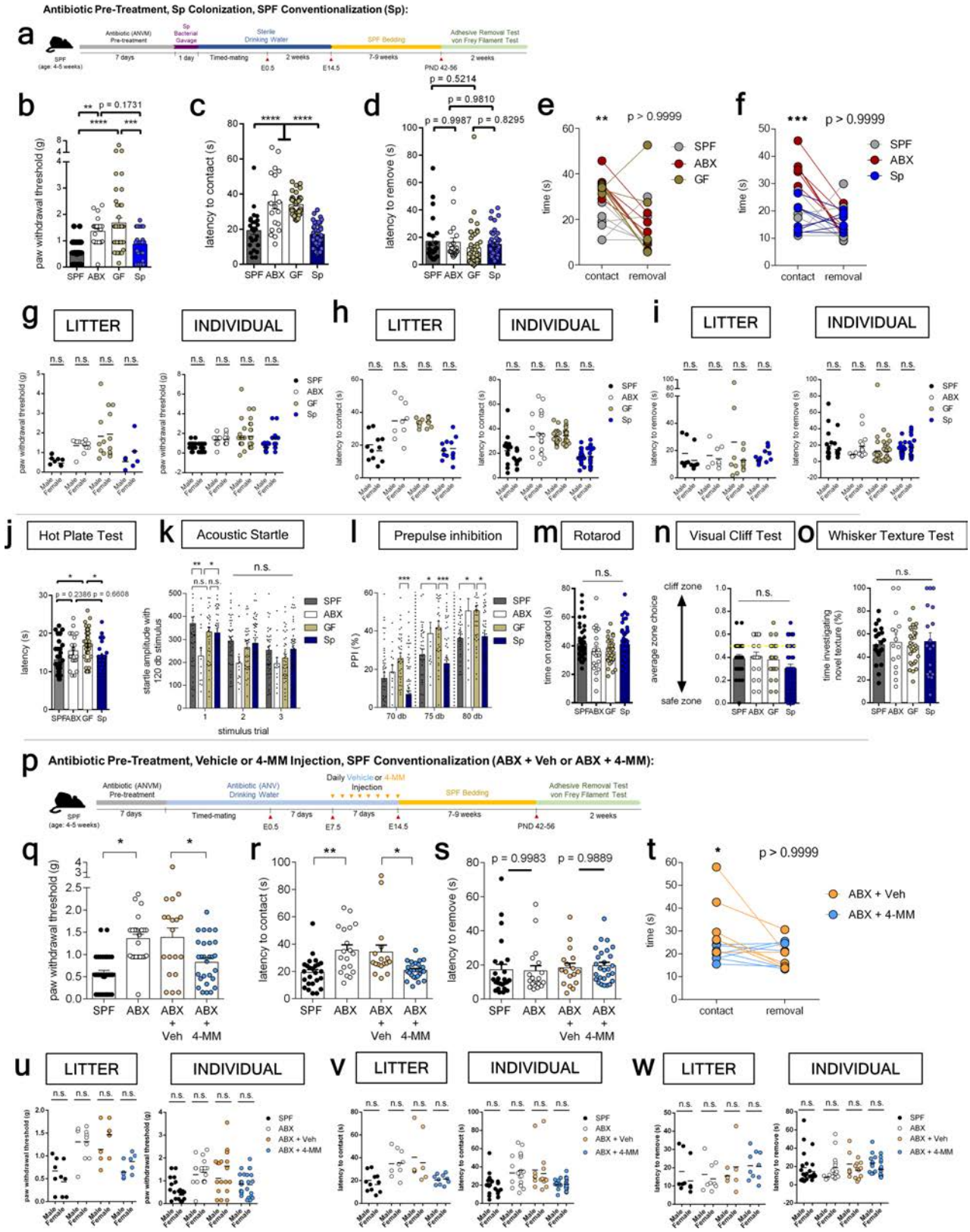

Extended Data Fig. 6 | See next page for caption.

Extended Data Fig. 6 | Effects of the maternal microbiome on behaviours. **a**, Maternal Sp colonization and SPF conventionalization. **b**, Force filament to induce 50% paw withdrawal (One-way ANOVA+Tukey's, $n = 38, 24, 45, 25$ offspring). **c**, Latency to contact the adhesive, and **d**, latency to remove adhesive after first contact (One-way ANOVA+Tukey's, $n = 35, 19, 45, 38$ offspring). **e**, **f**, Pairwise data for latency to contact and remove adhesive. (Two-way ANOVA+Sidak's, $n = 6, 6, 7, 7$ dams). **g**, Force filament to induce 50% paw withdrawal by sex, per litter or individual (Two-way ANOVA+Tukey's, $n = 5, 7, 7, 7$ dams). **h**, Latency to contact and **i**, remove adhesive after first contact (Two-way ANOVA+Tukey's, $n = 6, 6, 7, 11$ dams). **j**, Latency to withdraw from hot plate (One-way ANOVA+Tukey's; $n = 37, 19, 45, 25$ offspring). **k**, Habituation to acoustic tone (Two-way ANOVA+Tukey's; $n = 45, 25, 45, 52$ offspring). **l**, Inhibitory effect of prepulse on startle (Two-way ANOVA+Tukey's; $n = 45, 25, 45, 52$ offspring). **m**, Time on rotarod (One-way ANOVA+Tukey's; $n = 45, 20, 45, 50$ offspring). **n**, Visual depth discrimination. y = 0.05, equal instances of exiting safe vs. cliff zone. (One-way ANOVA+Tukey's; $n = 38, 19, 45, 52$ offspring). **o**, Percent time investigating novel texture (One-way ANOVA+Tukey's; $n = 20, 15, 29, 18$ offspring). **p**, 4-MM treatment and SPF conventionalization. **q**, Force filament to induce 50% paw withdrawal (One-way ANOVA+Tukey's, $n = 10, 23, 15, 21$ offspring). **r**, Latency to contact and **s**, remove adhesive after first contact (One-way ANOVA+Tukey's, $n = 25, 19, 15, 22$ offspring). **t**, Pairwise data for latency to contact and remove adhesive. (Two-way ANOVA+Sidak's, $n = 5, 5$ dams). **u**, Force filament to induce 50% paw withdrawal by sex, per litter or individual (Two-way ANOVA+Tukey's, $n = 5, 7, 5, 5$ dams). **v**, Latency to contact and **w**, remove adhesive after first contact. (Two-way ANOVA+Tukey's, $n = 6, 6, 5, 5$ dams). Data for SPF and ABX in **u**–**w** are as in **g**–**i**. $^{*}P < 0.05$, $^{**}P < 0.01$, $^{***}P < 0.001$, $^{****}P < 0.0001$. n.s. = not statistically significant. Number of dams, sex of offspring per group and behavioural task are detailed in Supplementary Table 3.

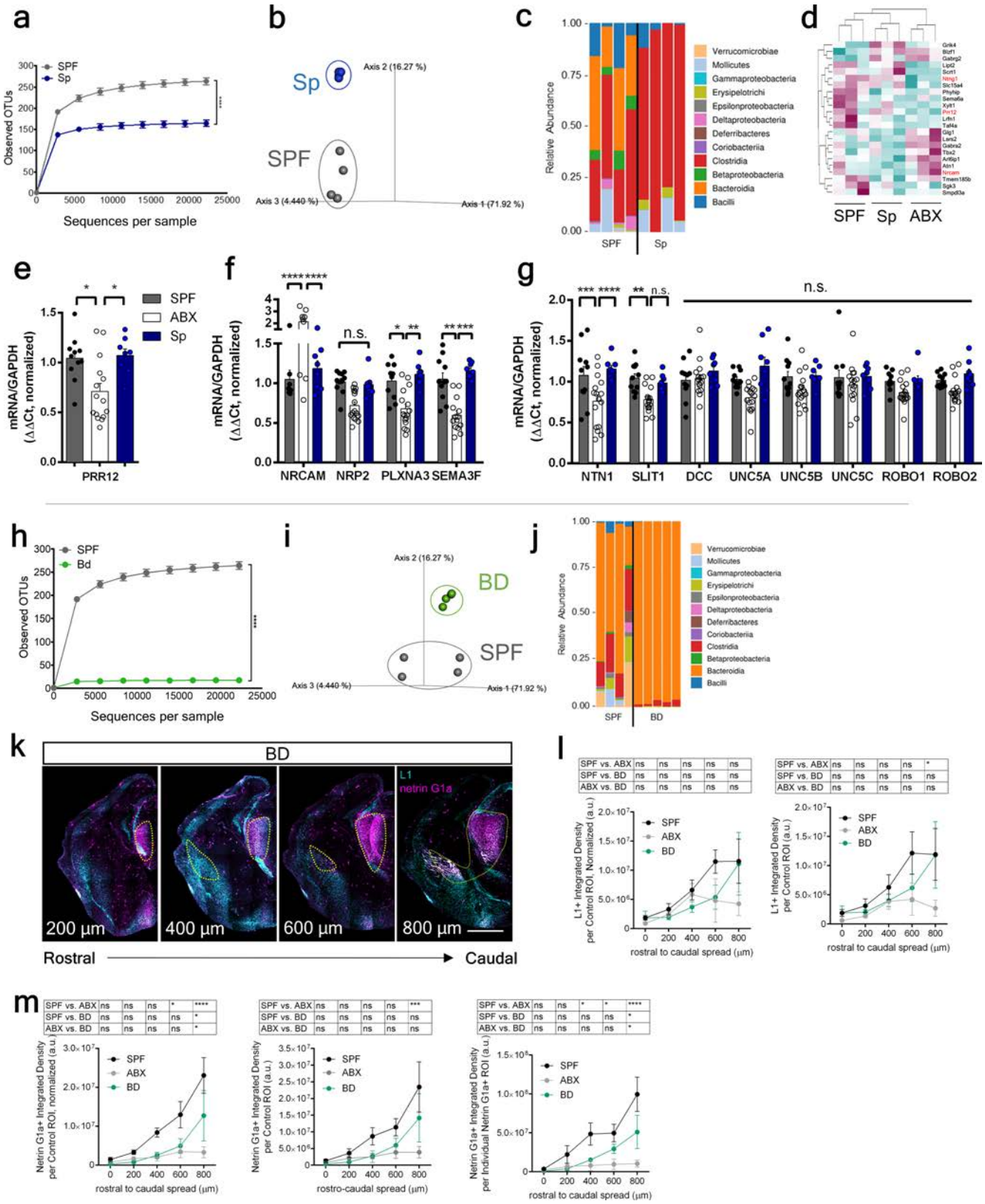

Extended Data Fig. 7 | See next page for caption.

Extended Data Fig. 7 | Maternal gut microbiota and fetal thalamocortical axons in dams colonized with a consortium of spore-forming bacteria or *Bacteroides*. Faecal microbiota of E14.5 SPF and Sp dams ($n = 4$ dams): **a**, rarefaction curves of observed operational taxonomic units (OTUs). **b**, Principal coordinate analysis of weighted sequencing data, and **c**, order-level taxonomic diversity. **d**, Genes commonly differentially expressed in E14.5 brains from offspring of SPF and Sp vs. ABX dams (two-tailed Wald, $n = 3$ dams). Data for SPF and ABX are as in Fig. 1. Red indicates axonogenesis-related genes. **e**, *PRR12* expression in E14.5 brains from offspring of SPF, ABX, and Sp dams (one-way ANOVA+Tukey's; $n = 11, 15, 8$ offspring). **f**, **g**, Expression of axonogenesis-related genes in E14.5 brains from SPF, ABX, and Sp dams (Two-way ANOVA+Tukey's; $n = 11, 16, 8$ offspring). Faecal microbiota of E14.5 SPF and BD dams ($n = 4, 5$ dams): **h**, rarefaction curves of the observed OTUs, **i**, principal coordinate analysis of weighted data, and **j**, order-level taxonomic diversity. **k**, Netrin-G1a (magenta) and L1 (cyan) in E14.5 brain sections of BD dams. Scale = 500 µm. Yellow lines = matched control ROI. **l**, L1 per matched control ROI, un-normalized (right) and normalized (left) by total brain area of E14.5 brain sections of SPF, ABX, and BD dams. Data for SPF and ABX are as in Figs. 1d and 2e, Extended Data Fig. 3g-i. (Two-way ANOVA+Tukey's, $n = 5$ dams). **m**, Netrin-G1a per matched control ROI, un-normalized (middle) and normalized by total area of E14.5 brain sections (left). Netrin-G1a in area of Netrin-G1a+ staining in E14.5 brain sections (right). Data for SPF and ABX are as in Figs. 1c and 2d, Extended Data Fig. 2. (Two-way ANOVA+Tukey's, $n = 5$ dams). Mean ± SEM. $^{*}P < 0.05$, $^{**}P < 0.01$, $^{***}P < 0.001$, $^{****}P < 0.0001$, n.s. = not statistically significant.

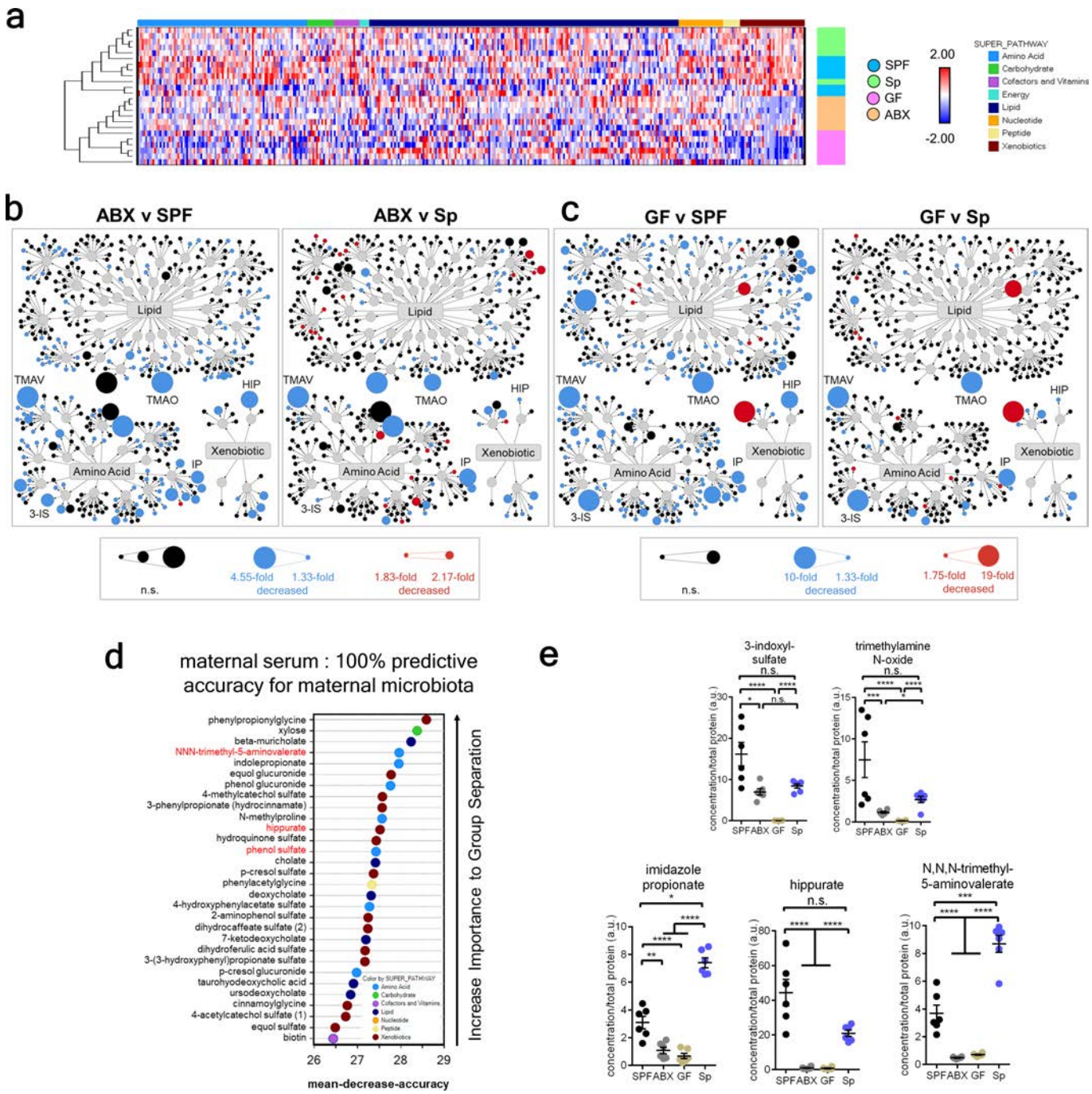

Extended Data Fig. 8 | Maternal serum and fetal brain metabolomic profiles from gnotobiotic dams. a, Unsupervised hierarchical clustering of 753 maternal serum metabolites ($n = 6$ dams). **b**, Amino acid, lipid and xenobiotic metabolites dysregulated in E14.5 fetal brains of offspring from ABX vs. SPF dams (left) and ABX vs. Sp dams (right) (q<0.05; One-way ANOVA, $n = 6$ embryos from different dams). **c**, Amino acid, lipid and xenobiotic metabolites significantly dysregulated in E14.5 fetal brains of offspring from GF dams vs. SPF controls (left) and GF dams vs. Sp dams (right) (q<0.05; One-way ANOVA, n = offspring from 6 dams per group). **d**, Random Forest classification of top 30 metabolites in maternal serum that discriminate between SPF and Sp vs. ABX and GF dams. ($n = 6$ dams). **e**, Relative concentrations of N,N,N-trimethyl-5-aminovalerate (TMAV), trimethylamine N-oxide (TMAO), imidazole propionate (IP), hippurate (HIP), and 3-indoxyl-sulfate (3-IS) in maternal sera of SPF, ABX, GF, and Sp dams (One-way ANOVA with FDR contrasts; $n = 6$ dams). Mean ± SEM. *q<0.05, **q<0.01, ***q<0.001, ****q<0.0001, n.s. = not statistically significant.

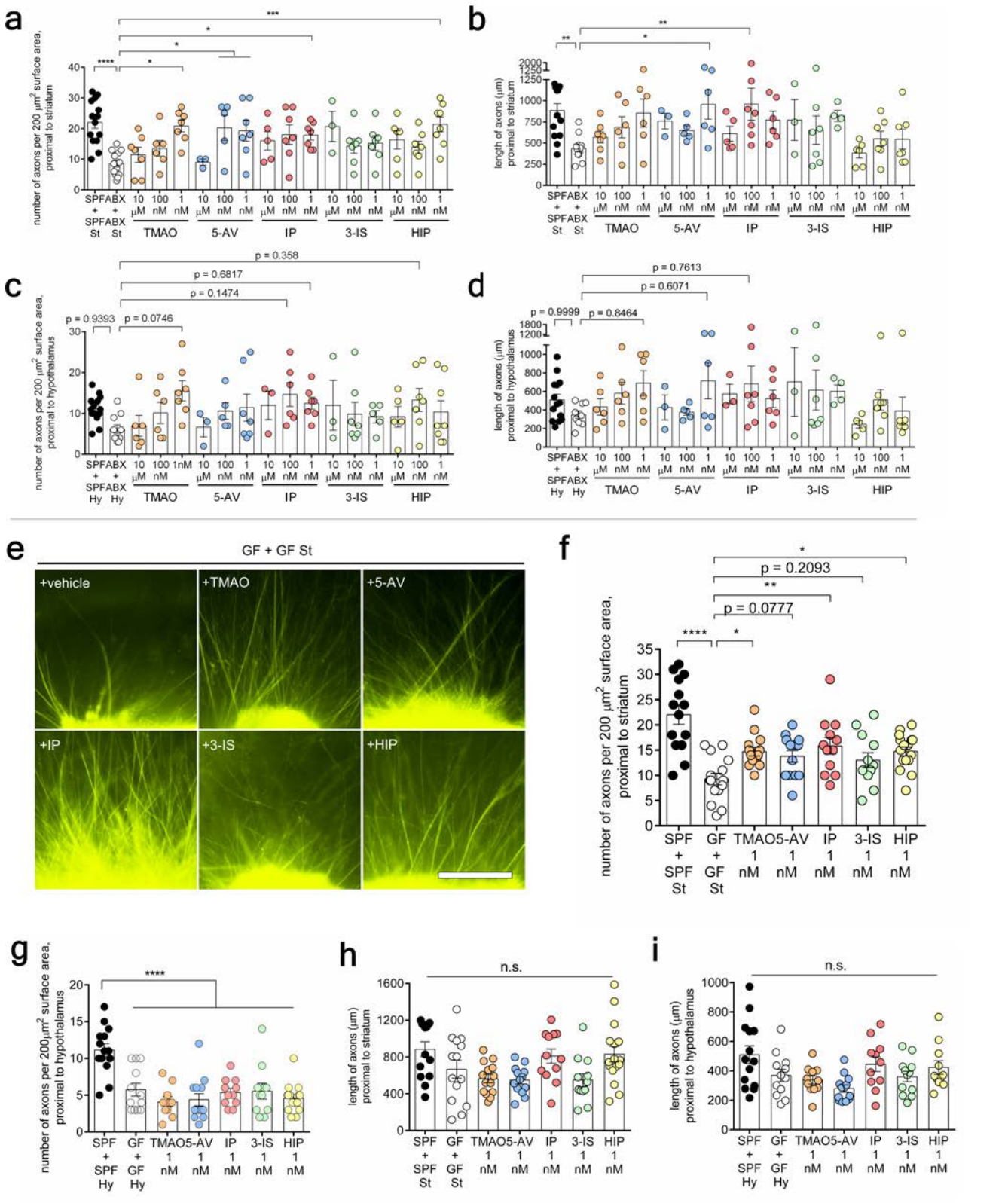

Extended Data Fig. 9 | Effects of microbiome-dependent metabolites on thalamocortical axon outgrowth from GF explant co-cultures. a, Axon number and **b**, axon length per 200 µm² surface area proximal to striatal explant (St) and from (i) SPF thalamic explant (Th)+SPF St (ii) ABX Th+ABX St, and (iii) ABX Th+ABX St, supplemented with 1 nM, 100 nM, 10 µM of metabolites: trimethylamine N-oxide (TMAO), 5-aminovalerate (5-AV), imidazole propionate (IP), 3-indoxyl-sulfate (3-IS) or hippurate (HIP). (One-way ANOVA+Tukey's, $n = 14, 13$, TMAO: 7, 6, 7, 5-AV: 3, 5, 7, IP: 5, 7, 7, 3-IS: 3, 7, 7, HIP: 6, 7, 8 explants). **c**, Axon number, and **d**, axon length per 200 µm² surface area proximal to hypothalamic explant (Hy) from (i) SPF Th+SPF Hy), (ii) ABX Th+ABX Hy, and (iii) ABX Th+ABX Hy, supplemented with metabolites. (One-way ANOVA+Tukey's, $n = 14, 10$, TMAO: 6, 6, 7, 5-AV: 3, 5, 7, IP: 3, 6, 7, 3-IS: 3, 7, 5, HIP: 5, 7, 8 explants). **e**, E14.5 GF Th proximal to GF St treated with metabolites. Scale = 250 µm. **f**, **g**, Axon number and **h**, **i**, axon length per 200 µm perimeter proximal to St (**f**, **h**) and Hy (**g**, **i**). (One-way ANOVA+Tukey's, $n = 14, 15, 14, 13, 12, 12, 16$ explants). Mean ± SEM. $^{*}P < 0.05$, $^{**}P < 0.01$, $^{****}P < 0.0001$.

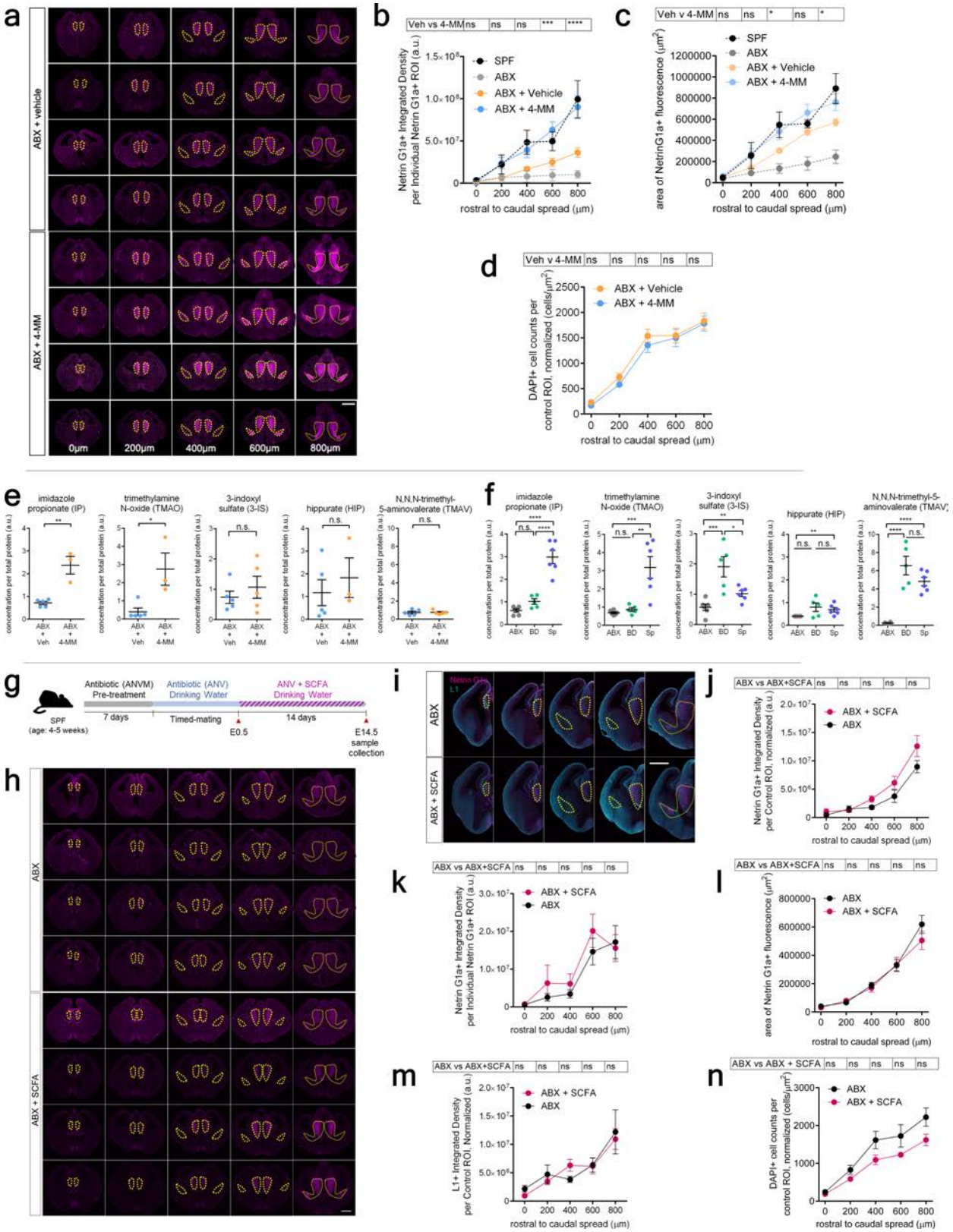

Extended Data Fig. 10 | See next page for caption.

Extended Data Fig. 10 | Microbiome-dependent metabolites in E14.5 brains after maternal supplementation with 4-MM or SCFA and effects on netrin-G1a thalamocortical axons. a, Netrin-G1a in four independent E14.5 brains from offspring of ABX+vehicle and ABX+4-MM dams. Scale = 500 µm, **b**, Netrin-G1a in area of Netrin-G1a+ staining in E14.5 brains from ABX+vehicle and ABX+4-MM dams. (Two-way ANOVA+Tukey's, $n = 8$ dams). **c**, Area of Netrin-G1a+ staining in E14.5 brain sections. (Two-way ANOVA+Tukey's, $n = 8$ dams). **d**, DAPI counts per matched ROI (yellow lines) normalized by total brain area. (Two-way ANOVA+Tukey's, $n = 4$ dams). **e**, Levels of the metabolites (i) imidazole propionate (IP), (ii) trimethylamine oxide (TMAO), (iii) 3-indoxyl-sulfate (3-IS), (iv) hippurate (HIP) and (v) N, N, N-trimethyl-5-aminovalerate (TMAV) in E14.5 brain lysates from antibiotic-treated dams supplemented with 4-MM or vehicle (One-way ANOVA, $n = 5$ (ABX+vehicle), 3, 3, 5, 3, 5 (ABX+4-MM) dams). **f**, Levels of IP, TMAO, 3-IS, HIP, and TMAV in E14.5 brain lysates from BD dams. (One-way ANOVA+Tukey's, $n = 6, 6, 5$ dams). **g**, SCFA administration. **h**, Netrin-G1a in four independent E14.5 brain sections from offspring of ABX and ABX+SCFA dams. Scale = 500 µm, **i**, Netrin-G1a and L1 in E14.5 brain sections from offspring of ABX and ABX+SCFA dams. **j**, Netrin-G1a per matched control ROI, normalized by total brain area. (Two-way ANOVA+Tukey's, $n = 4, 7$ dams). **k**, Netrin-G1a in area of Netrin-G1a+ staining. (Two-way ANOVA+Tukey's, $n = 4, 7$ dams). **l**, Area of Netrin-G1a+ staining. (Two-way ANOVA+Tukey's, $n = 4, 7$ dams). **m**, L1 per matched control ROI, normalized by total brain area. (Two-way ANOVA+Tukey's, $n = 4, 7$ dams). **n**, DAPI count per matched ROI, normalized by total brain area. (Two-way ANOVA+Tukey's, $n = 4, 7$ dams). Mean ± SEM. $^{*}P < 0.05$, $^{**}P < 0.01$, $^{***}P < 0.001$, n.s. = not statistically significant.

nature research

Corresponding author(s): Elaine Y. Hsiao, Helen E. Vuong

Last updated by author(s): Jul 1, 2020

Reporting Summary

Nature Research wishes to improve the reproducibility of the work that we publish. This form provides structure for consistency and transparency in reporting. For further information on Nature Research policies, see our Editorial Policies and the Editorial Policy Checklist.

Statistics

For all statistical analyses, confirm that the following items are present in the figure legend, table legend, main text, or Methods section.

n/a	Confirmed	
☐	☒	The exact sample size (*n*) for each experimental group/condition, given as a discrete number and unit of measurement
☐	☒	A statement on whether measurements were taken from distinct samples or whether the same sample was measured repeatedly
☐	☒	The statistical test(s) used AND whether they are one- or two-sided *Only common tests should be described solely by name; describe more complex techniques in the Methods section.*
☐	☒	A description of all covariates tested
☐	☒	A description of any assumptions or corrections, such as tests of normality and adjustment for multiple comparisons
☐	☒	A full description of the statistical parameters including central tendency (e.g. means) or other basic estimates (e.g. regression coefficient) AND variation (e.g. standard deviation) or associated estimates of uncertainty (e.g. confidence intervals)
☐	☒	For null hypothesis testing, the test statistic (e.g. *F*, *t*, *r*) with confidence intervals, effect sizes, degrees of freedom and *P* value noted *Give P values as exact values whenever suitable.*
☒	☐	For Bayesian analysis, information on the choice of priors and Markov chain Monte Carlo settings
☒	☐	For hierarchical and complex designs, identification of the appropriate level for tests and full reporting of outcomes
☒	☐	Estimates of effect sizes (e.g. Cohen's *d*, Pearson's *r*), indicating how they were calculated

Our web collection on statistics for biologists contains articles on many of the points above.

Software and code

Policy information about availability of computer code

Data collection	Image acquisition: Zeiss ZEN Blue and Black (2012), Leica DMi8 LasX, Behavior acquisition: Ethovision XT v11.5
Data analysis	Fetal brain transcriptomic analysis: FASTQC v0.11.8, HiSAT2 2.1.0, DESeq2 1.24.0, R studio, DAVID v6.8, STRING v10.5, pheatmap v1.0.12 16S rRNA gene sequencing: QIIME2 Image analysis: ImageJ (FIJI), Zeiss ZEN Blue and Black Editions, CTAn and CTVol software Statistical analysis: GraphPad Prism 6 Behavioral analysis: Ethovision XT v11.5

For manuscripts utilizing custom algorithms or software that are central to the research but not yet described in published literature, software must be made available to editors and reviewers. We strongly encourage code deposition in a community repository (e.g. GitHub). See the Nature Research guidelines for submitting code & software for further information.

Data

Policy information about availability of data

All manuscripts must include a data availability statement. This statement should provide the following information, where applicable:

- Accession codes, unique identifiers, or web links for publicly available datasets
- A list of figures that have associated raw data
- A description of any restrictions on data availability

All data generated and analyzed during this study are included in this published article and its supplementary information files. Source data for all figures are provided with the paper. The 16S rRNA gene sequencing data that support the findings are have also been deposited to the Qiita database with study IDs 13099, 13106 and 13107. Transcriptomic data that support the findings of this study have also been deposited to the Gene Expression Omnibus (GEO) repository with accession number GSE147183.

Field-specific reporting

Please select the one below that is the best fit for your research. If you are not sure, read the appropriate sections before making your selection.

☒ Life sciences ☐ Behavioural & social sciences ☐ Ecological, evolutionary & environmental sciences

For a reference copy of the document with all sections, see nature.com/documents/nr-reporting-summary-flat.pdf

Life sciences study design

All studies must disclose on these points even when the disclosure is negative.

Sample size	Group size estimates were determined by power calculation from current data and existing literature, and based on previous experience with the model system and experimental paradigm. Using our current data for population values and common standard deviation of SPF vs GF at 800um (mu1=3.85597e007, mu2=1.61649e007, sigma=6.196e006) along with a type I error rate of 0.05 and desired power of 0.80, we calculate that an n=3 would be needed to render the desired statistical power. Further, comparing exisiting literature of SPF v GF thalamic volume (Lu et al., 2018) that has mu1=9.26, mu2=8.64, sigma=0.22, a type I error rate of 0.05 and desired power of 0.80, we calculate that an n=3 would provide statistical power. Finally, drawing from other studies that measure fetal brain size in response to ethanol exposure, zika virus infection, and PDK1 genetic mutation, we see that typical sample sizes range from n=3 to 6 (Parnell et al., 2009; Zhang et al., 2019; Zurashvili et al., 2013). Applying the sigma values and mu values from Zurashvili et al., we see that the required n based on power calculation is n=4.
Data exclusions	No acquired data were excluded from experiments.
Replication	All experiments were replicated at least 3 times and all attempts were successful.
Randomization	Age- and sex-matched animals were randomly allocated into experimental groups.
Blinding	Investigators were blinded to experimental groups for prep and analysis : for 16S rRNA gene sequencing prep and analysis, fetal brain transcriptomic sequencing prep and analysis, netrin G1a and L1 IHC and PACT, and axon outgrowth image analysis, postnatal sensory behavioral assays and analysis.

Reporting for specific materials, systems and methods

We require information from authors about some types of materials, experimental systems and methods used in many studies. Here, indicate whether each material, system or method listed is relevant to your study. If you are not sure if a list item applies to your research, read the appropriate section before selecting a response.

Materials & experimental systems

n/a	Involved in the study
☐	☒ Antibodies
☒	☐ Eukaryotic cell lines
☒	☐ Palaeontology and archaeology
☐	☒ Animals and other organisms
☒	☐ Human research participants
☒	☐ Clinical data
☒	☐ Dual use research of concern

Methods

n/a	Involved in the study
☒	☐ ChIP-seq
☒	☐ Flow cytometry
☒	☐ MRI-based neuroimaging

Antibodies

Antibodies used	Primary antibodies: β tubulin III anti-mouse (1:500, EMD Millipore, Cat No. MAB1637), Netrin G1a anti-goat (1:100, R&D Systems. Cat No. AF1166) and Neural Cell Adhesion Molecule L1 anti-rat (1:500, EMD Millipore, Cat. No. MAB5272). Secondary antibodies: Donkey anti-goat (Cat no. A-11057), anti-rat (Cat no. A-21208) , and anti-mouse (Cat No. A-21202) secondary antibodies conjugated to Alexa Fluor 568 or 488 (1:1000, Thermofisher Scientific).
Validation	Concentration of antibodies were validated based on manufacturing instructions, serial dilutions, and omitting primary antibody controls. β tubulin III anti-mouse : https://www.emdmillipore.com/US/en/product/Anti-Tubulin-Antibody-beta-III-isoform-CT-clone-TU-20-Similar-to-TUJ1,MM_NF-MAB1637

Netrin G1a anti-goat: https://www.rndsystems.com/products/mouse-netrin-g1a-antibody_af1166

Neural Cell Adhesion Molecule L1 anti-rat: https://www.emdmillipore.com/US/en/product/Anti-Neural-Cell-Adhesion-Molecule-L1-Antibody-clone-324,MM_NF-MAB5272

Animals and other organisms

Policy information about studies involving animals; ARRIVE guidelines recommended for reporting animal research

Laboratory animals	Mouse C57Bl/6J, adult >8 weeks, males and females were used for breeding.
Wild animals	The study did not involve wild animals.
Field-collected samples	The study did not involve samples collected from the field.
Ethics oversight	All experiments were performed in accordance with the NIH Guide for the Care and Use of Laboratory Animals using protocol approved by the UCLA Animal Care and Use Committee (Experimental Protocol #: 2015-077).

Note that full information on the approval of the study protocol must also be provided in the manuscript.